國立交通大學

電子工程學系 電子研究所

博士論文

電阻式記憶體之特性研究及電性探討

The investigation on electrical characteristics and switching properties of resistive random access memory

研 究 生：曾文賢

指導教授：張國明　教授

劉國辰　教授

中華民國一〇〇年五月

電阻式記憶體之特性研究及電性探討

The investigation on electrical characteristics and switching properties of resistive random access memory

研究生：曾文賢　Student：Wen-Hsien Tzeng

指導教授：張國明　Advisor：Kow-Ming Chang

劉國辰　Kou-Chen Liu

國立交通大學

電子工程學系 電子研究所

博士論文

A Dissertation
Submitted to Department of Electronics Engineering and
Institute of Electronics
College of Electrical and Computer Engineering
National Chiao Tung University
in partial Fulfillment of the Requirements
for the Degree of
Doctor of Philosophy
in
Electronics Engineering

May 2011
Hsinchu, Taiwan, Republic of China

中華民國一〇〇年五月

電阻式記憶體之特性研究及電性探討

學生：曾文賢　　　　　　　　　　　　　　　　　　　指導教授：張國明
劉國辰

國立交通大學

電子工程學系　電子研究所

摘要

隨著可攜式電子元件的蓬勃發展，如手機及數位相機，非揮發性記憶元件在半導體產業的需求也日益增加。現今主流的非揮發性記憶元件為快閃式記憶體，然而快閃式記憶體存在一些必須克服的問題，如操作電壓較高、操作速度較慢以及記憶力隨元件尺寸微縮而降低等。因此新興的非揮發性記憶體也逐漸受到重視。在這之中，以電阻式記憶體(RRAM)最被看好。電阻轉換記憶元件具有操作電壓低、功率消耗低、操作速度快、可微縮性高、記憶時間長、耐久力佳及尺寸小、易和半導體製程匹配等優勢。RRAM是透過外加電壓或電流將氧化層決定至高或低阻值，以用以作為分辨0或1不同阻態之記憶體應用。然而，至今主要的轉態機制又依材料特性而異，而且影響RRAM的電性表現的效應至今依然有著探討的空間。

在此論文中，分別以二氧化鉿、三氧化二釓和鋁酸鑭材料來作為氧化層，並探討其在不同效應下的電性表現行為。這三種高介電材料是近年來閘極氧化層應用的候選材料。因此若能有良好的電阻轉態特性，則有利於1T1R在製程上的整合製作。探討的參數變因包含了本質的調變和外質的調變。本質調變參數有：上電極材料（鉑、鈀、鎳、鈦、鉭、鋁、鎢、鋁、氮化鈦）、操作模式（電壓驅動和或電流驅動）、操作極性（單極操作和雙極操作）、電極製程條件（電子束蒸鍍和濺鍍沉積）、沉積氧分壓條件、沉積溫度條件。而外質調變參數有：氮環境熱處理、氮氧環境中熱處理、紫外光效應。無論是單極操作或雙極操作的電性轉態行為，我們均提出可能的物理模型架構來解釋轉態機制，並且我們也能在

電性表現上有所提升和改善。

研究結果顯示，我們上述幾項研究變因參數皆會對轉態特性的好壞有所影響，而且氧化層和上電極之間的介面對於轉態特性的好壞扮演著極為重要的角色。選取適當的製程方式和製程參數，再搭配適合的上電極，我們能大幅提升單極操作的二氧化鉿的轉態特性。而當我們對介面進行處理，如照紫外光、以氟化氫溶液蝕刻表面、熱處理，皆得到相對較差的特性。我們的可逆實驗更加證實了介面的好壞可由我們人為的影響，來決定最後單極轉態電性的操作穩定性。在不同上電極材料的研究中，我們曉得二氧化鉿單極操作的特性是和上電極材料有關，更深入的研究，發現是上電極和氧化層之間所形成的中間層在主導著轉態電性的好壞。普遍接受的單極操作機制是，在 ON 操作時施加正偏壓將氧化層裂化，大量的氧離子被粹取至上電極介面。而 OFF 操作時，大量電流流過細小的細絲傳導路徑，產生高溫的焦耳熱，而因造成細絲路徑斷開，而回到高電阻態。因此，我們選取能提升二氧化鉿材料熱穩定性的材料鋁來作適當的添加，當二氧化鉿的熱穩定性被提升時，的確能有效的提升其在單極操作時的耐久度。在不同的熱處理和氧處理下，當介面的缺陷更加的被修復時，而造成細絲路徑的聚積，只是部份幾條細絲做傳導，因此在 ON/OFF 之間的切換更加的好控制，因此電壓散佈度也能有效的控制。而當氧化層表面受紫外光照射，或是電漿離子轟擊時，會造成氧化層表面的缺陷數量增加，如此會造成細絲路徑更加的散亂和任意的形成，因此會得到相對較差的轉態特性。

在雙極操作方面，我們也進行了研究。雙極特性的穩定與否，電極材料亦扮演著關鍵角色。正開負關或是負開正關的電阻轉態特性及其特性的穩定度，決定於介面層形成的好壞。我們以脈衝雷射沉積法(PLD)，來探討不同沉積溫度和氧分壓環境下所沉積的氧化層薄膜，其對於轉態特性的影響。研究成果顯示，在高溫下沉積的薄膜，其結晶性較好，表面的粗糙度變差，而在下電極和氧化層之間會有中介層形成。這層中介層也提供了氧的儲存槽的作用，以供氧離子能作來回的移動，因此會有較佳的電阻轉態的特性。施加負偏壓，將氧離子驅入至儲存槽中，因而路徑形成，轉態至 ON 態，施加正偏壓，將氧離子拉回氧化層中，因此路徑被修復斷開，轉態至 OFF 態。而在氧分壓高的環境中沉積，過多的氧原子會在沉積過程中反覆的和濺擊出來的沉積原子反應和碰撞，長成的薄膜結構較為緻密，可長成非晶態的鋁酸鑭氧化層。在氧分壓大中的環境沉積，能得到較粗糙的表面，薄膜和氧也鍵結愈強，表示氧空缺的量會大幅降低。而氧分壓大沉積過程易有碰撞，有些氧離子會被撞擊至試片表面，愈易造成中介層的生成。電性表現方面，在氧分壓大中沉積者有較大崩潰電壓、較低漏電流、較穩定的轉態特性及較佳的操作電壓散佈度。從電性傳導的角度，

來回推適合穩定RRAM操作的電性傳導應該為何。值得提出的一點是，我們亦成功的製作出透明的電阻式記憶體，克服了ITO電極不適合作為電極操作的問題。並擴展電阻式記憶體的可利用範圍。

The investigation on electrical characteristics and switching properties of resistive random access memory

Student：Wen-Hsien Tzeng
Advisors：Kow-Ming Chang
Kou-Chen Liu

Department of Electronics Engineering and Institute of Electronics
Nation Chiao Tung University

Abstract

Due to the popularity of portable equipment, such as mobile phone and MP3 player, the requirements of nonvolatile memory (NVM) increase significantly in the semiconductor industry. Flash memory is the mainstream among the nonvolatile memory devices nowadays, but several bottlenecks emerge, such as high operation voltage, low operation speed, poor endurance, and the scaling problem. The device dimensions are continuously scaled down, the flash memory faces the challenge of thin tunneling oxide that causes an unsatisfactory retention time. Therefore, the novel NVMs attract much attention in recent years. One of the promising candidates of next-generation NVMs is the resistive random access memory (RRAM) owing to its low operation voltage and power, high operation speed, high scalability, good endurance, small size, etc. However, the RRAM devices still exist many issues needed to be improved before the commercial application.

In this thesis, we investigated the electrical characteristics by using HfO_x, Gd_2O_3, and $LaAlO_3$ as the insulator layer. The three kinds of high-k dielectrics are the candidates that have been identified by the semiconductor industry as a potential replacement for SiO_2 in gate dielectric layers. Once these materials can exhibit reliable resistive switching properties, it can be a good choice for 1T1R integration application. The varying parameters we focus on including the intrinsic modulation (about metal-insulator-metal itself) and extrinsic modulation (post treatment). The intrinsic modulated parameters, such as top electrode material (Pt, Pd, Ni, Ti, Ta, Al, W, Cu, and TiN were used, respectively), operation mode (voltage bias operation or current bias operation), operation polarity (unipolar switching or bipolar switching), electrode

fabrication process (E-Gun deposition or sputtering deposition), oxygen partial pressure condition and deposition temperature and the extrinsic modulated parameters, such as thermal treatment in N_2, thermal treatment in N_2/O_2, UV light exposure effect, etc., were all discussed. For the unipolar and bipolar resistive switching characteristics, we both proposed the possible model to explain the switching mechanism. In addition, we can improve the electrical properties by modulating the above treatment.

The results reveal that the switching characteristics can be influenced by the modulated parameters listed above. In the investigation on electrical properties of HfO_x films by using different metal materials as top electrode, we observed that the unipolar switching characteristics are highly correlated to the top electrode materials. We further found that the interfacial layer formed between electrode and insulator film during deposition greatly dominates the switching properties. Based on the proposed unipolar switching mechanism, the general accepted model is the formation and rupture of the conducting filamentary paths, which is driven by the field for SET (OFF to ON) operation and thermal effect for RESET (ON to OFF) operation. We tried to improve the thermal instability of HfO_x by adding Al thin layer at the top insulator surface. Once the thermal stability of HfO_x was improved, higher thermal stability of HfAlO layer can effectively prevent the thermal noise against the unintentional stimulus, so the switching characteristics will be much better than that of other samples. In the study on post treatment, when samples are treated by oxygen gas at high temperature, defects at the surface will be oxidized and reduced. This can effectively confine the conducting filamentary paths to some local weak point, thus the random distribution of the conducting filamentary paths inside the insulator films can be avoided. The high and low resistance values can be greatly improved under the certain conditions of oxygen gas treatment. When samples surface were exposed under UV light (wavelength and laser intensity is about 365 nm and 80 mW/cm^2) or plasma ions bombardment, defect density at the insulator surface will be increased. Once the defect density increases, the filamentary paths tend to form in a random connection under the applied bias, so a much poor switching properties would be expected. We can modulate the defect density at the insulator surface by the depicted experiments above to control the resistive switching characteristics.

In bipolar operation, the electrode material also plays an important role to the bipolar switching properties. We also observed that the operation polarity depends on the interfacial layer. We investigated the process condition effect to the switching properties based on by pulsed laser deposition. Different process condition, such as deposition temperature and oxygen partial pressure, were experimented and discussed. The results reveal that when thin films

deposited at higher temperature, it has better crystallinity, larger surface roughness, and a thicker interfacial layer formed at the bottom electrode and insulator interface. The higher crystallinity can provide more grain boundaries inside the insulator films, which facilitate the migration of the movable oxygen ions. The interfacial layer can serve as a good oxygen reservoir for the oxygen ions rested under the negative bias. So, the state can be switched to ON state. When the positive bias was applied, the oxygen ions back to oxidize with the metallic defects inside insulator films, so the state was switched to OFF state. We also discuss the amorphous insulator films as the application for RRAM devices on $LaAlO_3$ thin films grown under different oxygen partial pressure. We clearly explain how different oxygen partial pressure influences the surface roughness, the formation of the interfacial layer, the leakage current density, the forming voltage and the transparent resistive switching characteristics of the $LaAlO_3$ thin films. The micro-structure and oxygen concentration different inside LAO thin films may be the main reason for the distinction of the electrical characteristics, as well as the resistive switching properties. LAO films grown at higher oxygen partial pressure is beneficial for a more reliable resistive switching performance, because the formation of the interfacial layer and lower oxygen vacancy concentration exist in the LAO thin film. Migration of the oxygen ions between the interfacial layer and the LAO films under applied bias may be the possible switching mechanism. We successfully fabricated the transparent RRAM (T-RRAM) based on Gd_2O_3 and $LaAlO_3$ thin films on glass substrate and extended the application of RRAM to the transparent electronics filed.

誌謝

首先我要感謝我的指導教授張國明教授，我才能順利的完成此博士論文。不論是在學術研究與待人處世上，都給予許多的指導與幫助。另外，我要感謝另一位指導教授長庚大學光電所劉國辰教授，在老師多年來耐心的教導之下，學到了許多實驗的研究方法，遇到問題學會去思考並且尋求解決之道，以及待人處世應有的腳踏實地與務實的態度，讓我博士班生涯受益良多。

感謝汪大暉教授、吳建宏教授、林鴻志教授、曾俊元教授、傅昭銘教授、趙天生教授及蔡銘進組長，於百忙之中撥空擔任我的論文口試委員，並對本論文提出許多寶貴的意見，使其更臻完善。

再來要感謝在這段研究生涯中，實驗室學長同學與學弟們的幫忙。感謝王敬業學長、賴瓊惠學姐、林稔杰學長、趙高毅學長、林俊銘學長、郭俊銘學長、林建宏學長、張知天學長、黃士軒學長、陳柏寧學長、陳巨峰學長等人的指導與協助。學長們的寶貴建議，不論在生活或研究上都給予了我許多關懷和幫忙。感謝黃菘宏學弟、張庭嘉學弟、何柏慶學弟在實驗操作、電性量測及物性分析上都給予了我很大的幫忙。感謝一起做研究的賴威仁學弟、吳天佑學弟、陳信宇學弟、詹宜竣學弟、郭俊志學弟、林煒力學弟、黃俊傑學弟、溫岳嘉學弟、張悳舜學弟和鍾嘉文學弟，這一路研究的辛苦我們一起走過，感謝你們的熱情努力付出。還有許許多多曾經幫助過我的人，感謝你們！

感謝交通大學電子工程研究所的各位教師多年來的栽培，對於每一堂課程如此盡心盡力的準備著教材，以期能給予我們最完整最詳盡的電子相關課程。感謝電子系所林明霓小姐、李清音小姐等許多的行政人員，幫我處理了多年有關報到、課程、註冊、成績、資格考、口試等相關煩瑣的問題。

感謝工研院電子與光電研究所的李亨元博士、陳邦旭博士及南亞科技公司Jengping Lin博士鼎力相助，提供設備機台及薄膜試片，也因此讓整個技術研究探討更為完整。尤其對我提出許多懇切的建議與想法，讓我獲益良多。感謝感謝中山科學研究院的何炎騰博士、淡江大學物理系葉炳宏教授，提供製程設備以供我研究與探討電性。

感謝交通大學奈米中心以及國家奈米實驗室在實驗器材上的大力支持，能讓

我有完善的儀器設備與環境來達成的我的實驗。感謝清大、交大、中央、中興貴儀中心提供分析設備幫忙物性分析。

最後，我要感謝我親愛的父母親、姊姊春萍及女友僑妘，你們一路無悔的默默支持我念完博士班，給予我物質上和精神上的支持與關懷，讓我無後顧之憂能全心全意朝自己的夢想大步邁進。

謹以此論文獻給每一個關心我、愛我的人。

Contents

Chapter 1 Introduction

Chapter 2 Experimental details

Chapter 3 Results and discussion of the resistive switching

properties in the HfO_x-based memory devices

Chapter 4 Results and discussion of the resistive switching properties in the Gd_2O_3-based memory devices

Chapter 5 Results and discussion of the resistive switching

properties in the LaAlO-based memory devices

Chapter 6 Conclusion

Table Caption

Chapter 1

Figure Caption

Chapter 1

Chapter 3

Chapter 4

Chapter 5

Chapter 1 Introduction

1.1 Introduction of Memory

Memory can be easily divided into two main categories: volatile and nonvolatile. Volatile memory loses data when the applied bias is turned off. A constant power is required to maintain the stored data. There are two main types of random access memory (RAM), namely, dynamic random access memory (Dynamic Random Access Memory, DRAM) and static random access memory (Static Random Access Memory, SRAM), that belong to this category (Figs. 1.1 and 1.2, respectively). The unit size of a DRAM cell is composed of a transistor and a capacitor (1T1C). It has only a small device size (6-12F^2) [1] in which high device density and high capacity can be achieved on a DRAM array cell. Therefore, DRAM has a lower cost per bit than memories with less compact array, in addition to faster access speed, giving it a high performance rating. However, the charge decays away in a finite length of time (milliseconds); a periodic refresh is needed to restore the charge for a DRAM to retain its memory. As for a conventional SRAM cell (50-80F^2) [2], it consists of a basic flip-flop circuit that needs only a DC current applied to retain its memory. It contains four transistors plus either two transistors or two polysilicon-load resistors as pull-up devices (Fig. 1-2). No periodic refresh is required, thereby eliminating the need for external address counters and refreshing circuitry used in DRAM. Nevertheless, SRAM is larger than a basic cell, which makes it more expensive to build, has higher power consumption because DC power should be applied continuously, and, historically, has a slower speed.

1.1.1 Nonvolatile memory

Nonvolatile memory included read only memory (ROM), electrically programmable read only memory (EPROM), and electrically erasable programmable ROM (EEPROM). NVM does not lose stored data when the power is turned off. ROM is preprogrammed in a silicon by the semiconductor manufacturer using a program pattern supplied by an ROM user. ROMs have the advantages of being manufactured using a relatively low technology and inexpensive process. Conversely, aside from the fact that their contents cannot be altered, ROMs require a high initial, one-time cost to produce a custom product. On the other hand, EPROM has provided a solution to address the erasable requirement. EPROM has a cell containing a select and a storage transistor that holds excess charge when programmed, which can be erased and reprogrammed by the user. EPROMs are more expensive than ROMs in per-unit cost for volume quantities, but are a solution to the need for a reprogrammable nonvolatile memory. However, there are several disadvantages to EPROMs. They are not as fast in performance as RAMs or ROMs, and they cannot be reprogrammed in the system. Normally, they must be removed from the system manually and reprogrammed using special ultraviolet (UV) light equipment to erase the old programming followed by another piece of equipment to program the new. EPROMs are in ceramic packages with quartz windows that can be damaged by automated insertion equipment and thus must be hand inserted in the sockets.

The shortcomings of EPROM have been overcome by a relative newcomer to the memory arena, EEPROM. EEPROM can be electrically erased in the system; thus, the need to buy expensive ultraviolet erase equipment is eliminated. EEPROMs are available in standard plastic packages without the quartz window, which eliminates light-sensitivity problems and enables the EEPROMs to be inserted in high-volume applications using an automated insertion equipment. It also erases considerably faster than EPROM, that is, a few milliseconds is needed for EEPROM, whereas half hour is required for EPROM. However, the memory density of EEPROM is lower than that of EPROM. This shortcoming limits the application of EEPROM to lower storage capacity equipments only. Several variations of this technology include metal nitride oxide semiconductor (MNOS), silicon oxide nitride oxide semiconductor (SONOS), floating gate tunneling oxide (FLOTOX), and textured polysilicon.

Flash memories based on EPROM or EEPROM technologies are devices for which contents of all memory array cells can be erased simultaneously, unlike the EEPROMs that have select transistors incorporated in each cell to allow for the individual byte erasure. The mainstream NVM today in the market is flash memory, which provides wide application and a technology driver for the global semiconductor. Flash memories include NOR flash and NAND flash, and provides the functionality of different products requirements. NOR flash is more suitable for code storage applications, such as mobile phones and DVD players. NAND flash has higher density and is used for data storage market for emerging applications, such as PDA, memory cards, MP3 audio players, digital cameras, and USB flash personal discs. An additional gate called floating gate was embedded between the poly gate and the gate oxide in the traditional metal-oxide-semiconductor field effective transistor (MOSFET) invented by S. M. Sze and D. Kahng in 1967 [3]. The structure of the conventional floating-gate device is shown in Fig. 1-3. The floating gate can store electrons and is electrically governed by a capacitively coupled control gate. By controlling the numbers of injected electrons inside the floating gate, different threshold voltage of the flash memory can be obtained. This method is used to determine different states, which is based on whether charges are stored in the floating gate or not.

Recently, however, some bottlenecks of flash memory have been identified, such as high operation voltage, low operation speed, and poor retention time. To improve the switch speed of a flash memory, the thickness of tunnel oxide must be reduced.

The tunnel oxide of the conventional flash memory must maintain an appropriate thickness to provide superior isolation under retention, endurance, and disturbed conditions to keep the data storage invariable for 10 years. Hence, there is a tradeoff between switch speed and reliability for the optimum thickness of tunnel oxide. Some advanced flash memories, such as charge-trapping flash and band-engineered SONOS flash, have been proposed to satisfy the continuous shrinking demand [4,5]. Currently, several groups are eagerly finding the emerging next-generation NVMs that have high density, high speed, and nonvolatility. There are four possible candidates for the next-generation NVMs: ferroelectric random access memory (FRAM) [6-8], magnetroresistive random access memory (MRAM) [9-11], phase change random access memory (PCRAM) [12-14], and resistive random access memory (RRAM).

1.1.2 Next-generation NVM

(a) FRAM

FRAM is a NVM based on the ferroelectric effect of the charge storage mechanism, and is quite different from the floating-gate-based NVM. Typical perovskite ferroelectric materials are $BaTiO_3$, $PbTiO_3$, PZT ($PbZr_{1-x}Ti_xO_3$), PLZT ($Pb_{1-x}L_xZrO_3$), PMN ($PbMg_{1-x}Nb_xO_3$), SBT ($SrBi_2Ta_2O_9$), SBN ($SrBi_2Nb_2O_9$), and among others. The ferroelectric effect is the ability of a material to store an electric polarization in the absence of an applied electric field. A FRAM device cell is fabricated by depositing a ferroelectric film in crystal form between two electrode plates to form a capacitor. The perovskite crystals of a ferroelectric material maintain two stable polarization states resulting from the alignment of internal dipoles, corresponding to states of logical “1” and “0,” which in turn reverses the alignment of these internal dipoles. A simplified model of a ferroelectric crystal is shown in Fig. 1-4(a) [6]. A mobile atom is in the center of the crystal, and application of an electric field across the face of the crystal causes this atom to move in the direction of the field. A reversal of the field causes the atom to move in the opposite direction, resulting in a typical hysteresis curve, as shown in Fig. 1-4(b). The positions of the atom at top and bottom of the crystal are stable, and the atom remains in these states when the external field is removed. No external electric field or current is required for the ferroelectric material to remain polarized in either state; hence, a memory device can be built for storing digital (binary) data that will not require power to retain information stored within it. The critical temperature for ferroelectric materials is known as the Curie temperature; the perovskite structure assumes a cubic symmetry and is paraelectric when the Curie temperature is exceeded, that is, the films will lose the ferroelectric behavior. Therefore, the Curie temperature for a ferroelectric material must be high enough to maintain a wide margin of the application in semiconductor technology. The polarization versus temperature curve is shown in Fig. 1-4(c) [7,8].

To read a FRAM, detecting the position of the atoms within the petrovskite crystals is necessary. However, it cannot be directly sensed. The read operation involves applying an electric field across the capacitor, causing the mobile atoms to move across the crystals in the direction of the field if they are not already in the appropriated positions. The circuit dumps charge resulting from the applied field from the capacitor and compares it to the charge from a reference. A capacitor with atoms that switch states will emit a larger charge than a capacitor with atoms that do not switch. The memory sensing circuitry must determine which capacitors switched. The "switched charge" allows the circuit to determine the state of the memory cell. Given that a memory read operation involves a change of state, the FRAM circuitry must restore the original memory state. Therefore, each read access is accompanied by a pre-charge operation that restores the memory states. To write a FRAM, no system overhead is required, and the operation is very similar to a read operation. The circuit applies write data to the ferroelectric capacitors, and the new data switches (if necessary) the state of the ferroelectric crystals.

(b) MRAM

MRAM is solid state, nonvolatile magnetic storage device in which the stored data are represented by the magnetization direction and the readout is done by resistance measurements. According to the proponents of MRAM, this technology scales better to low voltages than DRAM, SRAM, and flash memories, and it requires fewer mask steps than the DRAM process. Early MRAMs were based on the anisotropic magnetoresistance (AMR) effect. Only less than 5% of the amplitude of the AMR effect in thin films limits the application only to military and space application. In 1988, the discovery of the giant magnetoresistive (GMR) effect [9] changed this situation. This GMR technology (5-15%) has been applied in commercial products like hard disk drive (HDD) read heads and magnetic sensors. A breakthrough in the field of magnetic tunnel junctions was achieved sometime in 1995, when the large tunnel magnetoresistive (TMR) effect [10] was demonstrated at room temperature, further contributing to the development of MRAM. The TMR has the potential of reaching MR ratios of 30-40%. However, a tougher challenge lies in finding the right process recipe that would enable the production of reliable MRAMs.

In general, both GMR and TMR result in low resistance if the magnetization directions in the multilayer are parallel, and in high resistance when the magnetizations are anti-parallel. For the representation of storage bits, different possibilities exist. The pseudo-spin valves use two ferromagnetic layers that switch their magnetization direction at different magnetic fields, which can be accomplished by utilizing layers of different magnetic materials, or layers of the same material but of different thicknesses. A typical structure of MRAM cell is shown in Fig. 1-5.

The resistance of two thin ferromagnetic layers separated by a thin nonmagnetic conducting layer can be altered based on whether the moments of ferromagnetic layers are parallel or anti-arallel. The layers with parallel magnetic moments will have less scattering at the interface, longer mean free paths, and lower resistance. On the other hand, the layers with antiparallel magnetic moments will have more scattering at the interfaces, shorter mean free paths, and higher resistance. In order for the spin-dependent scattering to be a significant part of total resistance, the layers must be thinner than the mean free path of electrons in the bulk material. For many ferromagnetic materials, the mean free path is tens of nanometers, so the layers themselves must each be typically less than 10 nm.

The addressing of the MRAM is done using an array of crossing lines. Writing a certain cell is equivalent to setting a magnetization in the desired direction. By applying a current pulse to a bit line and a word line, lines experience the maximum magnetic field, thereby reversing its magnetization. All other MRAM cells below the bit or word line are exposed to the significantly lower field that is caused by a single current pulse and, therefore, will not change their magnetization directions.

(c) PCRAM

The phase-change memory technology stores information using structural phase changes in certain thin-film alloys. The semiconducting properties of a range of crystalline and amorphous chalcogenide alloys were investigated in the early 1950s. Up to date, the chalcogenide is a proven phase-change material used in the rewritable CDs and DVDs [11]. The operation of PCRAM devices is based on the principle that the films can be designed to be highly resistive semiconductors in the amorphous phase and highly conductive semimetals in the crystalline phase [12]. These alloys should be stabilized in the crystalline state (in Fig. 1-6(a)) in which the atoms are arranged in a regular periodic structure, as well as in the amorphous state (in Fig. 1-6(b)) with irregular atomic state [13,14]. The phase-change alloys are referred to as the chalcogenide materials. These two structural states have different optical and electrical properties, and two states by application of electric pulses of energy sufficient enough to overcome the energy barrier separating the two states.

The phase-change conversion is accomplished by appropriate heating and cooling of the material. A laser beam pulse energy is used to detect these structural phase changes. On melting, the material loses its crystalline structure; and rapidly cooling it below its glass transition temperature results in the amorphous phase. To keep the material from recrystallizing during cooling, the cooling rate must be faster than the crystal nucleation and growth rate. To switch the memory cells back to the conductive state, the material is heated to a temperature between the glass transition temperature and the melting temperature, causing the nucleation and crystal growth to occur rapidly, as shown in Fig. 1-6(c).

(d) RRAM

RRAM devices like PCRAM, based on different resistance state to distinguish the high or low state; these devices have emerged recently and are considered to be promising candidates of NVM. Unlike PCRAM, which exhibits homogeneous change on the resistance values inside the thin film, the change in resistance values in RRAM devices only occur at some certain localized positions among the insulator. Only a several nm order of the filamentary path in diameter is needed to perform a successful resistance switching. Therefore, RRAM devices can offer great advantages of small cell size, excellent scalability and high density array. A simple fabrication process for RRAM devices is compatible with the standard semiconductor technology. Furthermore, the voltage values required to switch RRAM devices are quite low, sometimes in the range of approximately 1-3 V to accomplish a sufficiently large resistance difference, which exhibits low operation voltage and high-to-low resistance ratio. At present, a RRAM array with high speed operation, long endurance and retention time has been performed, verifying the high potential of the RRAM applications. Several oxide materials, such as binary metal oxides, perovskite-based oxide, chalogenide materials, solid-state electrolytes, and organic molecular materials, have been proposed to exhibit resistive switching (RS) properties, thereby showcasing the flexibility of RRAM devices.

1.2 Resistive switching phenomenon

Resistive values, triggered by applying voltage/current bias or pulse to different resistance values; they were first discussed several decades ago. These properties include the forming process phenomena, which is an essential and irreversible change in conductivity induced by a high electric field (Fig. 1-4). After forming, negative resistance (NDR), as well as switching and memory phenomena, is observed. These properties are demonstrated in a wide range of semiconductor materials, including amorphous or microcrystalline binary insulators prepared under certain appropriate conditions with suitable thickness or fabrication process. The basic structure of RRAM is composed of a metal-insulator-metal (MIM) or metal insulator semiconductor (MIS) stacked capacitor. Systems which show NDR have the following performed behaviors: current-controlled (S-type) and voltage-controlled (N-type) types, which imply that resistance change is triggered by applying current or voltage bias, as shown in Figs. 1-7(a) and (b).

1.2.1 Unipolar operation

Devices under different sweeping directions may obtain distinct electrical behaviors. Two main categories of electrical behaviors, namely, unipolar and bipolar operation, have been reported and investigated in recent years. Unipolar operation denotes that the applied voltage used to trigger the resistive switching is based on the same polarity of voltage bias, that is, both by positive or negative bias. A typical unipolar electrical curve is shown in Fig. 1-8. After the electroforming process, the state is then switched to LRS. When the positive bias is re-applied, the electrical properties follow Curve 2 with a larger conducting current than the unformed sample. Until the applied voltage reaches a certain voltage value, a sudden decrease in current value is observed, and then the state is switched to high resistance state (HRS). As the positive bias is applied again, the current values - which are about 1 or 2 orders lower than the low resistance state (LRS), but are still higher than the unformed sample - increase gradually. Continuous increase in the applied voltage to a certain voltage value (Curve 1) results in an abrupt increase in the current. At this moment, the state is switched back to LRS. Two different conducting current values can be used as two different resistance states, namely, HRS and LRS, which are fundamental to RRAM devices. The voltage values which the state changes from HRS to LRS and LRS to HRS are denoted as the set voltage (V_{set}) and the reset voltage (V_{reset}), respectively, whereas the switch process is called the SET and the RESET process. In some reported studies, unipolar RS is also called as nonpolar RS.

1.2.2 Bipolar operation

Bipolar RS depicts that the RS phenomenon is observed by applying a specific polarity of voltage or current bias to reach the LRS state, or back to the HRS state by applying another polarity of the voltage or current bias [Figs. 1-9 (a) and (b)]. Bipolar switching can be performed by the following two sweeping current loops: clockwise and counterclockwise current loops. The clockwise current loop indicates that a device is switched to LRS by negative bias and back to HRS by positive bias. Conversely, the counterclockwise current loop shows the opposite operation process, that is, positive bias for SET and negative bias for RESET. This type of switching is also named as polarity-dependent RS, which means that the formation and rupture of the filamentary paths are both related to bias polarity.

1.3 Unipolar Resistive switching

The basic structure of RRAM is composed of an MIM, where "I" dominates the insulator film. The "M" is the metal electrodes, which can be extended to the low-resistivity electron conductor and sometimes for the ion conductor. In recent years, transparent conducting oxide (TCO) materials, such as indium tin oxide (ITO), fluorine doped tin oxide (FTO), and indium zinc oxide (IZO), have also been used as top electrodes for RRAM devices. Generally, a conducting filamentary path composed of defects is generated under the applied voltage/current bias inside the insulator matrix. The reliability of RS is determined by whether the switching is accurate. Once the conducting path can be formed and broken stably and reproducibly, the RS reliability will then be greatly improved. However, the resistive switching is highly dependent on the materials, including both electrode and insulator films, which make understanding the properties of RS more difficult. Consequently, during the beginning of research in this field, the switching mechanisms between two different materials often contradict each other. Currently, many issues or factors have been discussed in determining the relationship between either switching parameters. The two operation types, namely, unipolar or bipolar RS, are often investigated separately because they have different needs on their respective demands and different switching mechanisms. Unipolar RS has a simple circuit design and higher cell density, which demonstrate its high potential for application. Nevertheless, the stability and reliability of unipolar RS essentially need to be improved further to achieve the demands of commercialized NVM applications. On the other hand, bipolar RS can be switched reproducibly and reliably, which is based on the migration of trapped electrons, oxygen ions, oxygen vacancies, or ionized cations under different polarities of applied bias, to trigger to ON and OFF states. In the following sections, we discuss the characteristics of RS, as well as its reported effects, factors, treatment conditions, and improvement techniques.

1.3.1 Rupture phenomenon

The NDR phenomenon has been observed on SiO_x, Ta_2O_5, Nb_2O_5, and Al_2O_3, among others, since the 1960s, and several possible forming process and resistive switching mechanisms have been investigated in the early days. Hickmott et al. [15] reported that some high-field-dependent processes reduced the number of impurity centers and contributed to conduction (e.g., neutralization from hole centers). The schematic diagram of their proposed model is shown in Fig. 1-10. Simmons and Verderber [16] constructed an impurity band in the center of an insulator film, and proposed that once the impurity band falls below the anode, the current would decrease because only the electrons below the top of the impurity band contribute (Fig. 1-11). Dearnaley et al. [17] reported that filaments are characterized by two important features. The first feature is that the filament may fracture and cease to contribute to conduction; the second is that the filament can re-form under suitable conditions, and the re-forming will be related to the basic forming process of propagation of the filament through the insulator. The fracture of the filament is probably a consequence of Joule heating, which raises the temperature of a part of the filament so that there is local atomic reorganization, as in melting or other phase changes. When continuously operated, the two features exhibit the RS behavior. Dearnaley’s model has frequently been adopted to explain switching characteristics; however, the tiny difference between materials is still unknown due to the lack of precise measurement and analysis techniques. Their model is too rough to use in elucidating the development of mainstream NVM in the specific investigation. In the last decade, many groups have deeply investigated and observed the microcrystalline and microstructure of thin films based on the relationship of RS. In the following sections, we examine the occurrence of the thermal Joule heating effect.

(a) Thermal Joule heating

The RESET process of unipolar RRAM devices based on the thermal Joule heating effect is mainly used to explain this mechanism. A high thermal temperature arises from high current density, althrough the existing defects inside the TMO films may induce high Joule heat under applied bias. Resistance change based on thermal Joule heat has been observed in many TMO materials. Kim et al. [18] roughly estimated the temperature of formed filaments using the steady state temperature model, where the equation for which is given by $T_m = \left(T_o^4 + \frac{J^2 \rho r}{2 P_w} \right)^{1/4}$, where T_m is the filament temperature raised by Joule heating, T_o is the room temperature, J is the current density, ρ is the sample resistivity, r is the filament radius, and P_w is the radiative loss parameter for the filament (which is about 3×10^{-7} W m^{-2} K^{-4}). A temperature more than 720 K can be estimated roughly by assuming the current of 200 nA of a Ni nanowire with r = 5 nm and ρ = 5×10^{-4} Ω cm. Sato et al. [19] investigated the switching behaviors of TMO junction by applying a single short-voltage pulse. Form the results, the authors proposed a thermal chemical reaction model of the reset mechanism. The resistance R of the filament is assumed to follow Ohm’s law. The heating temperature is given for a typical filament by

$\Delta T = \frac{1}{(K_R + K)} \frac{V_{reset}^2}{R}$. Thus, the dependence between heating temperature and radius of filament with different resistivity values can be represented, as shown in Fig. 1-12; for example, for a Ni filament with ρ = 30 μΩ cm and r = 20 nm, the heating temperature is approximately 1000 °C. Chen et al. [20] proposed that the temperature effect can be linked to the thermal release time of trapped charges, and the field effect can be attributed to a field-induced barrier lowering. On the basis of the field-induced barrier lowering effect from $\Delta E \alpha \sqrt{qF/\pi\varepsilon}\,(eV)$, the erasing temperature can be estimated to be ~800 °C. He et al. [21] studied the switching mechanism of carbon-based RRAM. They simulated the heat generation and propagation driven by an electric current pulse during the switching process; the authors reported that the temperature was approximately 2200 K when set to low resistance, and 4000 K when the state was switched to high resistance. The reported estimated heating temperature is summarized in Table. 1.

(b) Thermal rupture model

Russo et al. constructed a SET and RESET model based on experimental and numerical analysis data; the authors discussed the filament conduction properties and RESET transition kinetics characterization for NiO-based RRAM devices [22]. Using the physics-based numerical modeling of the RESET operation based on conductive filament (CF), they evaluated a statistic characterization of critical filament temperature for the RESET operation. Their results are consistent with a thermally activated RESET mechanism and support a diffusion-based model for RESET. Based on simulation data, the RESET transition was self-accelerated as a consequence of a positive feedback between the thermal dissolution of the CF and local Joule heating in the CF bottleneck, which was used to account for the abrupt resistance transition in experimental data [23]. The study of Russo et al. [22] was further investigated by Cagli et al. [24], who addressed the analytical modeling of SET and RESET processes in NiO-based RRAM cells. The SET model is based on threshold switching as the initiating mechanism of the transition to low resistance, while the RESET model assumes a thermal dissolution/oxidation of the low-resistance conductive filament.

(c) Where to rupture

Understanding where the filamentary path is to be formed and ruptured is important because the properties of RS during switching depend on the formation and rupture of the conducting filamentary paths. It can be easily divided into two categories: bulk dominates or interface dominates. Russo and Cagli believed that the major heating takes place close to the middle of the CF due to the approximately parabolic temperature profile in the CF during the applied electrical bias. As a result, the disconnection of CF occurs in correspondence with the middle of the filament [20,22,23]. By simulating the heating that takes place within vicinity of the M/O interface, their proposed model can also be well fitted. The simulation on RS has been shown by He et al. [21] to be the illustrated filament breakage and regrowth, as well as its related temperature distribution (Fig. 1-13). A different outlook was proposed to depict where to rupture based on Kinoshita’s report. Kinoshita et al. [25] investigated the data retention properties of NiO films exposed to sputtered particles and thermal stress. The authors found that the retention of the HRS data is dependent on the polarity of the bias voltage used to program the data, and that RS takes place on the anodic side of the conductive filaments. Kim et al. [26] first compared the RS properties of TiO_2, Al_2O_3, Al_2O_3/TiO_2, and $Al_2O_3/TiO_2/Al_2O_3$ thin films by I-V measurements using Pt/insulator/Ru structures. The authors observed that the layer that is secondarily encountered by the injected electrons controls the overall switching characteristics, suggesting that the first layer always remains in LRS during the entire switching cycle. They further investigated on a Pt/40 nm TiO_2/Pt capacitor structure and proposed that the conducting filaments propagate from the cathode interface to the insulator film [27]. Moreover, they argued that RS is induced by the rupture and recovery of the filaments in the localized region approximately 3-10 nm thick near the anode. Their model can also explain well the noisy Ohmic behavior once the voltage bias is applied as opposed to the last operation performed [28]. Only a certain part of the filaments near the anode electrode, and not the whole filament, actively contributes to switching. In their subsequent experiments, they observed that when W and Ir metals were used as top electrodes, the RS property was quite different. They also connected W tip/NiO/Ir/NiO/W tip sample serially and measured the I-V curve, and arrived at the opposite conclusion that the rupture of the conducting filaments occurs at the cathode side while the anodic side is still conducting [29]. Such findings imply that the electrodes may be another dominant factor in the RS operation. Several studies have reported that the oxide film near the anode electrode in some TMO films, such as NiO [18], TiO_2 [19], Cu_2O [20], HfO_x [30] will dominate the RS. However, recent direct experimental results in support of the location of the CF rupture are not available.

(d) Thermal instability

Thermal instability is one of the considerable issues for unipolar RRAM; the main RS mechanism is based on the field induced for SET and thermal Joule heating for RESET process. The applied voltage can be controlled from the measurement setup or a suitable compliance current; however, measuring the accumulated thermal heat during each RESET operation by electronic devices is not possible. Hence, controlling the suitable Joule heat during a RESET process to accomplish a stable switch to a certain HRS is a critical issue for unipolar RRAM. In 2005, Rohde et al. [31] first reported the RS of 43 nm-thick TiO_2 thin films by electric-pulse-induced operation; the common result obtained was a changing energy but with constant power necessary for one switching event, indicating that RS is a power-induced mechanism. Yun et al. [32] investigated the nanometer-sized localized filaments on the surfaces of NiO films by conductive-AFM; the authors observed the each spot, which is assumed to indicate the beginning of the localized conducting filaments, can be created or destroyed in a random manner (Fig. 1-14). Chang et al. [33] examined the effect of thermal dissipation on RS properties. The thermal instability of the conducting filaments induced the resistance memory switching phenomena to unstable and threshold switching (Fig. 1-15). Variations in CF parameters arise from local variations in material composition – for example, stoichiometric variations in NiO_x filaments, metallic impurities, diffused from the electrodes, and structural defects - may as well be a critical issue in causing fluctuations in switching behaviors (Fig. 1-16) [34].

1.3.2 Influence factors

As previously mentioned, the random nature properties of the formation and rupture of CF may be related to fluctuations in the thermal Joule heat during the RESET process. In this section, we discuss the reported factors influencing unipolar RS properties and ways to improve them. The schematic diagram of an MIM stacked structure is illustrated in Fig. 1-17. Three parts of the basic stacked structure MIM have been investigated in detail to study the relationship between the two parameters. Moreover, the buffer layer, which is an additional layer inserted at the top electrode (TE)/insulator, at the middle insulator, or at the insulator/bottom electrode (BE), can determine the final RS properties. Doping impurities with additional atoms by implanted or annealing can improve the switching performance. Some researchers utilized embedded metal nanoparticles inside TMO film to enhance the switching properties. External factors such as annealing or treatment are also performed.

(a) TMO films

A TMO film is a mother of an RRAM device because it is the main portion of an MIM capacitor and greatly depends on thin-film properties, such as atomic composition, crystalline phase, grain size, grain structure, and surface roughness, among others. The microstructure of thin films significantly depends on the fabrication process. Many candidate materials have been proposed to exhibit RS characteristics, including binary metal oxides (TiO_2, NiO, ZrO_2, Cu_2O, HfO_2, ZnO, CeO_2, Gd_2O_3, Al_2O_3, Ta_2O_5, CoO, MgO, Fe_2O_3, Nb_2O_5, WO_x, MoO_x, etc.), perovskite-type oxide [$SrTiO_3$ (STO), $SrZrO_3$ (SZO), $LiNbO_3$ (LN), $PbTiO_3$ (PTO), $Bi_4Ti_3O_{12}$ (BTO), $PbZr_{0.2}Ti_{0.8}O_3$ (PZT), and La_2CuO_4], carrier-doped manganites with perovskite structure, colossal magnetoresistance [$Pr_{1-x}Ca_xMnO_3$ (PCMO), $La_{1-x}Ca_xMnO_3$ (LCMO), $La_{1-x}Sr_xMnO_3$ (LSMO), and $Nd_{0.7}Ca_{0.3}MnO_3$ (NCMO)], and organic materials. Solid-state electrolytes materials, such as SiO_2, Ta_2O_5, CuS, GeS, GeSe, and WO_3, among others, can also be used as electrolytes to perform the RS properties.

A variety of fabrication processing techniques can be used for the deposition of TMO thin films, such as dc sputtering, rf sputter, e-beam evaporation (E-Gun), atomic layer deposition (ALD), plasma-enhanced atomic layer deposition (PEAVD), electron cyclotron resonance (ECR) sputtering, plasma-enhanced chemical layer deposition (PECVD), pulsed laser deposition (PLD), metallorganic chemical vapor deposition (MOCVD), sol-gel method, and anodization reaction method, among others. Metal thin film deposition, followed by metal oxidation through furnace and/or plasma oxidation, can demonstrate RS behaviors.

Several fabrication conditions for various fabrication techniques have been investigated. Among these are the following: film thickness, sputtering power, oxygen contents, background pressure, in-sputter deposition, film thickness, substrate temperature, and oxygen partial pressure in PLD process; and film thickness, substrate temperature, and reactive resource in ALD process. Given that the conducting filamentary paths for the RS operation are tiny and are highly related to the microcrystalline, microstructure, grain size, grain structure, surface morphology, and atomic compositions of the TMO films, a slight variation induced from the fabrication process may cause a considerable distinction on the RS properties.

(b) Top electrode

Despite the fact that the proper location to rupture the conductive paths at highest thermal heat is still being debated, the properties of thin films at the M/I interface may regulate the injected carriers and dominates the electrical characteristics. These properties include contact resistances, M/I barrier, interface states density, trapped charges carriers, and interfacial dipole, among others, may have a significant role in determining the final electrical conduction. The metal thin film has its specific work-function (WF), electron affinity, and Gibbs free energy for oxygen, as well as the different contact properties, when in contact to different insulator films. Recent reported issues such as Fermi-level pinning (FLP) or charge neutralization level (CNL) model may induce a complex M/I interface before and after the applied bias. In the succeeding paragraphs, we summarize the reported effect of top electrodes on the switching properties of various oxide films.

Seo et al. [35] investigated RS in top-electrode/NiO/Pt structures in which the top electrode was Au, Pt, Ti, or Al. When the metal/insulator interface was an ohmic contact (e.g. Pt/NiO/Pt and Au/NiO/Pt structures), the effect of the electric field inside the film was high enough to induce trapping/detrapping at defect states, thereby resulting in RS. For a Ti/NiO/Pt structure with a well-defined Schottky contact at the Ti/NiO interface, no RS was observed because the effective electric field inside the NiO film was not large enough (Fig. 1-18). Spiga et al. [36] investigated NiO and Nb_2O_5 thin films deposited by e-beam evaporation (E-Gun) and atomic layer deposition (ALD), respectively. In NiO films, the different bottom electrodes evidently influenced the programming voltages, which could be related to the different work function of the used bottom electrodes and the resulting oxide/electrode contact. Among the various bottom electrodes, such as n^+-Si, Pt, W, and TiN, better results in terms of number of cycles were obtained for noble metal and for the n^+-Si bottom electrode. In Nb_2O_5 films, the worse performance of the device was observed in W bottom electrodes, which may be correlated with the formation of a thin not-controlled WO_x interfacial layer. Lee et al. [37] examined NiO films, and reported that electrode dependence on RS did not result from the work function of the metal electrode/NiO contact, but rather was a result of the free energy of metal oxide formation compared to Ni oxidation. Based on Ellingham diagram (Fig. 1-19), an additional metal oxide formed at the metal/oxide interface affected the RS characteristics due to the metal oxide breakdown that occurred at the anodic side. Although the location to rupture the conducting filaments is still controversial, distinct electrical properties were observed among different M/I interface. The electrode plays an important part in switching properties whenever the Joule heating occurs.

(c) Buffer layer or inserted metal at the M/I interface

The M/I interface is key to determining the switching properties of RRAM; thus, once an additional layer is inserted at the M/O interface, the switching characteristics can be modulated. This additional fabrication process is sometimes used to improve RS characteristics, in which the switching parameters are sometimes fluctuant. Kim et al. [38] reported that inserting thin IrO_2 layers at M-I interfaces is beneficial in minimizing the dispersions of memory switching parameters. Go et al. [39] investigated the M/O interface based on Pt/Si/TiO_2/Pt structure by inserting a Si interlayer with a thickness ranging from 5 to 20 nm between Pt and TiO_2 films. The authors reported that the insertion effectively increases the adhesion of Pt to TiO_2, as well as resulted in a significant improvement in reliability with regard to the duration of the RS cycles and device yield. In addition, the insertion modulated the dispersion of switching parameters. Choi et al. [40] examined the RS properties of double-layer NiO/SiO_2 films with varying additional SiO_2 layer thickness; a very high on/off ratio, reliable retention, and cyclic switching characteristics were achieved by inserting a SiO_2 layer at the NiO/Pt interface. Lee et al. [41] reported that inserting an oxygen-riched NiO_y layer between electrode/insulator interface to form a multilayer structure of NiO_y/NiO_x/NiO_y (where $y > x$) improved the switching behaviors. Considering the switching mechanism through the formation and rupture of conducting filamentary paths inside TMO films, an additional interfacial layer can modulate the RS properties. This method is an effective way to improve unstable and unreliable switching parameters.

(d) Inserted metal inside the bulk TMO

Song et al. [42] reported that inserting thin Al metal layer inside AlO_x films improved the resistance switching properties of AlO_x-based RRAM devices. The endurance, as well as the resistance values and operation voltage fluctuation, were all considerably enhanced, which may be due to the effective number of increased localized active regions and the fact that SET and RESET processes can occur at certain localized regions before the total breakdown.

(e) Doping impurity

Impurity doping in electron devices modifies their electronic transport, and can be used to improve their performance. Tsunoda et al. [43] proposed that a drastic improvement of t_{reset} to less than 5 ns can be achieved by doping Ti into the NiO film. Moreover, the authors argued that the Ti-doped NiO memory exhibits the advantages of low-power (< 3 V) and small reset current (100 μA). Doping the Ti into the NiO film enhanced the population and diffusion of oxide ions during the RESET process, resulting in a stable anodization with fast speed using a large reset voltage. Jung et al. [44] investigated the effect of lithium (Li) doped in polycrystalline NiO film. The authors observed that Li-doping improved the off-state thermal stability in doped NiO films, resulting in a better retention property in the off-state and stable on/off operation. Liu et al. [45] reported that the switching characteristics of TiO_2-based memory devices improved by doping Gd in TiO_2 thin films. The authors argued that Gd-doping may induce the formation of oxygen vacancies and modify the oxygen vacancy distribution within the TiO_2 films, further leading to better RS characteristics. Liu et al. [46] investigated $Au/Cr/Au^+$-implanted-ZrO_2/n^+-Si sandwiched structure, and observed that the implantation of Au ions improved RS characteristics. Liu et al. [47] adopted the Cu-doping method to improve switching dispersion. The addition of Cu ions inside the NiO_x can increase the possibility of forming and connecting conducting filaments.

(f) Thermal Treatment

Samples under surface treatment can alter the film composition, crystallinity, thickness, interfacial layer, and/or oxygen ions and vacancies distribution, which in turn enhance the reliability of RS characteristics. Phark et al. [48] investigated the RS behaviors of NiO films using Pt or Ag as bottom electrodes. Chemical analyses revealed that the NiO/Ag (NiO/Pt) interface underwent an irreversible (reversible) reaction during heat treatment in a vacuum and oxygen environment. Their results suggest that the metal/oxide interfacial reaction may play an important role in RS phenomena. Chen et al. [49] observed that BFO films annealed at 500 °C and 550 °C showed unipolar switching behaviors, whereas those annealed at 450 °C did not. From the variation of the ohmic conduction, this result indicates that the carrier concentration in the BFO film increases with the annealing temperature, and the possible defect traps are oxygen vacancies. Panda et al. [50] investigated the switching characteristics of Pt/NiO/Pt memristive devices under different post-annealing temperature from 200 to 500 °C. The set voltage increased rapidly with the anneal temperature due to the formation of a larger cluster, whereas the reset voltage did not change as much. The resistance ratio of HRS to LRS for the annealed samples was enhanced with the annealing temperature. Mao et al. [51] tuned the forming voltage to be compatible to the set voltage by controlling the thickness and post-annealing temperature of ZnO thin film. The authors found that the forming voltage and microstructure grain size as a function of annealing temperature can be obtained to perform the forming-free RS phenomenon of Cu/ZnO/n^+-Si device. Kwak et al. [52] reported the Pt/CoO_x/Pt structure post-annealed at 400 °C performed a reproducible and reliable unipolar switching up to 1000 cycles, as opposed to the un-annealed with only 57 switching cycles. The authors found that the post-annealed samples may reduce the excess oxygen and the crystalline defects in the CoO_x layer. Moreover, they suggested that the reduction behavior of oxygen atoms inside the CoO_x may be an improvement factor for reliable switching properties.

(g) Other factors

Other factors that influence RS properties have been investigated, including photo-induced NDR effect, plasma damage, UV irradiation, and ammonia solution treatment, to name a few. Chen et al. [53] investigated the photo-enhanced NDR and photo-accelerated time-dependent dielectric breakdown (TDDB) in thin nitride-oxide (NO) dielectric film under tungsten (W) lamp illumination. Kinoshita et al. [25] observed that the data retention of NiO films was lost once the anodic side of the TMO films was exposed under plasma condition while the cathodic side was not. Tzeng et al. [54] investigated the effect of UV light on RS characteristics, as well as to the thin film properties of the ITO and HfO_2 films. The authors found that UV-light exposure can enhance oxygen-related defects or oxygen vacancies inside the HfO_x film, which results in the formation of some percolated conducting filaments near the grain boundaries; moreover, an oxygen-rich HfO_2 layer formed at the M/O interface effectively modulate the switching properties and reduce the dispersion on switching parameters. Liu et al. [55] investigated the RS of the $Al/Cu_xO/Cu$ structure, and found that the transition from HRS to LRS can be induced by dc voltage application, ultraviolet illumination, or thermal heating.

1.3.3 Switching stability improvement

(a) Switching parameters

One of the unipolar RS issues is the random fluctuation of the resistive switching parameters, such as V_{set}, V_{reset}, R_{off}, and R_{on}. R_{off} and R_{on} are the resistance values used to represent the high and low resistance states, and V_{set} and V_{reset} are the required voltages values to trigger the switching of a RRAM device. The operated voltages and resistance values are highly correlated each other during one cycle of switching. Once one of the four terms disperses, the determined values will be altered, and the next operation will be also changed. It would cause severe problems in controlling and reading the RS states. It seems no solution for this thorny problem in the beginning of the unipolar RRAM research. However, many researches have tried to find out the methods to suppress the RS variations recently. Some of the additional process we discussed above showing the benefits of improving the switching characteristics, including inserting buffer layer or metal layer at the M/O interface [38-41], inserting metal layer in the middle of TMO film [42], dopping impurity [43-47], and thermal treatment [48].

Baek et al. [56] improved the cycling distribution by using smaller active memory area to reduce the number of possible current paths in TMO films and the current paths do not vary much. Kim et al. [38] reported the improvement in minimizing the dispersion of all memory switching parameters using thin IrO_2 layers between NiO and electrodes. The roles of IrO_2 on top of Pt can enhance the crystallinity of NiO on top with fine microstructures at NiO-IrO_2 interfaces, which help to stabilize the local oxygen migrations for the filament formation and rupture, thus resulting in more stable memory switching parameters. Lee et al. [57] enhanced the switching parameters dispersion by controlling the composition of the top electrode. Ni migration from electrode into the NiO layer will effectively decrease the thickness of NiO film and enhance lightning rod effect due to the decrease of the thickness/roughness spacing ratio, as shown in Fig. 1-20. In addition, the contents of Ni metal inside NiPt electrode should be well controlled. Jung et al. [58] showed the failure-free NiO_x film directly grown on Pt electrode just by process control during NiO deposition. The existence of the defective structure composed of local Ni-Pt phase at the Pt/NiO interface provides powerful information about stable resistance switching properties. Choi et al. [40] modulated the RS properties by inserting SiO_2 layer in NiO memory devices, a very high on/off ratio (10^5), reliable retention, and cyclic switching characteristics were achieved. From TEM analyses, the formation of the metallic filaments inside SiO_2 layer is responsible for the RS behaviors. Among the reported papers, we may conclude that defect exists in the vicinity of the anodic electrode can efficiently improve RS characteristics, such as switching parameters, endurance, retention, and reliability. It is one of the beneficial ways to be adopted.

(b) Current reduction

A large conducting current during the RESET process is sometimes needed to induce the Joule heat to break the conducting filamentary paths. However, this may cause large power consumption during the operation for a memory array application since the memory is composed of high density of memory cells. Therefore, it is very important to keep the maximum on-state current (reset current, I_{reset}) as low as possible. Seo et al. [59] fabricated a NiO-20%/NiO-5%/NiO-20% stacked layer in order to reduce on-state current. Because the conduction of NiO-5% is higher than that of NiO-20%, a conductivity switching only inside a NiO-5% layer with high resistance and keeping two NiO-20% layers in off states in the same thickness. Tsunoda et al. [43] fabricated the Ti-doped NiO films and investigated the relationship between current compliance values and reset current. The I_{reset} can be greatly reduced with reducing the current compliance in the 1T1R integrated structure, while no dependence was observed in a two-terminal measurement (1R). The effect of an embedded series transistor acts as an excellent current limiter in the set process. Their extended investigation [60] compared R_{off} and reset current as a function of Vg with a 4 μm and 0.36 μm-gate-width transistor and a very low reset current of only 55 μA was obtained in 0.36 μm devices. The reason for this low reset current is that the superior current limit by using a selected transistor is effective with the filamentary conductive type. Fang et al. [61] achieved a reset current of 20 μA using $Cu/Cu_2O/Ni$.

They claimed that the switching mechanism of the Cu_2O resistive memory was relevant to space-charge-limited conduction (SCLC), which are dependent on the number of trapped charges. The memory cell integrated with a selected transistor – voltage-clamp transistor, can act as a current limiter, therefore, the overshoot of voltage or current bias can be minimized. The high to low resistance ratio is sometimes improved with the dispersion of switching parameters decreased, because the dispersion of the resistance values of high and low resistance states may minimize the resistance distribution. Therefore, the reports we discussed above can enhance the resistance ratio beneficially.

1.4 Bipolar resistive switching

The bipolar switching operation attracts much attention in recent years owing to its reliable switching behaviors, and stable operation than that of unipolar switching. A specific characteristic nature of merely migrated electrons, ions, vacancies, or charged defects under the different polarity of applied bias, makes them to be stable switching properties. The proposed model to explain the switching characteristics varied from samples to samples, and some of them even utilize the combined model to elucidate the RS behavior. In this section, we will first introduce the proposed switching mechanism, and explain the possible switching behaviors. From a microscopic point of view, resistance switching in various materials can be classified broadly into three different mechanisms. One is fuse-antifuse mechanism, in which the filamentary paths are created through the insulator matrix under an applied bias and are fused as a result of Joule heating. The other is the electrochemical metallization mechanism, which relies on an electrochemically active electrode metal such as Ag and Cu, causing the high drift mobility of Ag^+ and Cu^+ cations dissolution and reduction inside the insulator matrix. Amorphous selenides and sulfides acts as solid electrolytes are sometimes used. The others is the valence change memory, which based on variation of a transition of anions as a result of migration of the oxygen ions/vacancies. Many groups have built up the participation of impurities as essential for the RS in recent years. An accumulation or a depletion of these oxygen ions/vacancies or impurities will affect the valence states of the transition metal cations and may cause a considerable change in the electronic conductivity. The RS between high resistance state (HRS) and low resistance state (LRS) has been attributed to the formation and rupture of the filamentary conductive path consisting of different types of defects, which is highly related to its microstructure, such as crystallinity, grain structure, and atomic composition.

1.4.1 Bipolar switching mechanism – Thermal Joule heating

Though the thermal Joule heat under applied bias is mainly used to explain the unipolar RS behavior as we discussed in 1.3.1 section, however, some bipolar RRAM devices also observed this phenomenon. Tang et al. [62] investigated resistive switching characteristics, temperature effect, and electrode-size dependence on the Al/CuO_x/Cu device. They suggested that the electrode-size dependences of the LRS and the HRS can be explained in terms of conductive filament formation and the contribution of Joule heating. Chen et al. [63] based on Cu_2O MIM resistive memory and reported that power is a critical factor in erasing, which may be related to the thermal effect of power dissipation during erasing. Yin et al. [64] discussed the role of Joule heating on the Al/Cu_xO/Cu films during RESET process. Using the dc voltage sweeping method, the device can be operated by both bipolar and unipolar switchings. For RRAM devices, once the bipolar switching behaviors belong to this category, they may exhibit the nonpolar characteristics. The relationship between unipolar and bipolar, i.e. the nonpolar electrical properties, will be discussed in next paragraph.

1.4.2 Bipolar switching mechanism – Electrochemical metallization

This kind of switching cell, based on the electrochemical metallization effect, also called conductive bridging (CB) cells or Programmable metallization cells (PMC) in the literature. An electrochemical metal deposition and dissolution is utilized to perform this type of switching. It needs the electrode made from an electrochemically active metal M, such as Ag, Cu, or Ni, the noble metal, such as Pt, Ir, W, Au on the another side, and a solid electrolyte types of thin film, such as GeS, GeSe, and CuS, sandwiched between both electrodes. Some groups also performed the CB switching properties by using the Cu-doped TMO thin film. The electrochemical process follows the listed three steps: (i) anodic dissolution of active metal M according to the reaction ($M \rightarrow M^{z+} + z^{e-}$), (ii) the M cations migrate across the solid-electrolyte thin film under the applied bias, (iii) reduction and electrocrystallization of M on the inert electrode side according to the chemical reaction ($M^{z+} + z^{e-} \rightarrow M$) [65]. The illustrated picture is shown in Fig. 1-21 and Fig. 1-22. In 1976, Hirose et al. [66] first fabricated the Ag/Ag-As_2S_3/Au stacked structure with Ag-doped As_2S_3 thin film as solid electrolyte and observed the formation of a single Ag filament under an optical micrograph. This kind of switching memory exhibits quite low operation voltage, fast switching speed, and large resistance ratio. However, high temperature effect and retention issue may be the key problems needed to be improved.

As we summarized the proposed switching properties in this category, the main material used for the operation is based on using Cu and Ag top electrode. Some of the TMO thin films may be doped with Cu ions to enhance the Cu ions contents inside TMO films. Although they all belong to this type of RS, however, some details of the switching mechanism are different between each other. Cu/HfO_2/Pt by Haemori et al. [67] and Cu/AlN/Pt by Chen et al. [68] reported the un-doped TMO thin film and explained that the two resistance states might be related with the rupture and generation of filaments composed of thermally diffused Cu ions, in which a model concerning redox reaction is involved. The redox reaction character of Cu ions can also be driven into the amorphous carbon thin film to form Cu metallic filaments inside it, as the Cu/a-C:H/Pt structure reported by Zhuge et al. [69], and exhibit the switching properties under the opposite applied bias. Sometimes, the solid electrolyte materials may be used as the un-doped TMO thin film, such as Cu/Ta_2O_5/Pt by Sakamoto et al. [70], Au/Cu/$Ge_{0.2}Se_{0.8}$/W and Cu/$Ge_{0.4}Se_{0.6}$/W by Rahaman et al. [71,72], then the resistive change may be attributed to Cu metal precipitation in the solid electrolyte by an electrochemical reaction. And the multilevel state can be performed by modulating the compliance current. Ono et al. [73] reported a resistive switching ion-plug memory with a solid electrolyte layer that has Cu ions and resistive switching layer. They use a Cu-Ta-S film not a Cu for the supply layer because the amount of Cu supply can be controlled by Cu concentration in Cu-Ta-S. This can well prevent the extra Cu ions penetration and result in higher endurance than that of other Cu-based solid electrolyte memory.

When additional Cu atoms are doped inside TMO thin film, the electronic current may tunnel via Cu clusters within the oxide. Cu/Cu:SiO_2/W by Thermadam et al. [74], Pt/Cu:MoO_x/Cu by Lee et al. [75] and Ir/Cu:SiO_2/Cu by Schindler et al. [76] proposed the doped-TMO material and reported that the electrochemical formation and dissolution of a Cu filament is the switching mechanism for their device.

The following devices use two combined switching mechanism to explain their RRAM device. Liu et al. [77] fabricated the Ti/Cu:ZrO_2/n^+-Si structure and observed three distinguishable resistance states. From the temperature-dependent measurement results, they proposed that filaments due to ionic trap-controlled space charge limited current conduction and metallic bridge are formed in parallel at different voltages.

Yang et al. [78] investigated the switching mechanism of Cu/ZnO/Cu/ZnO/Pt resistive memory before and after anneal treatment at 700 °C for 30 s. They observed the RTA treatment has triggered a switching mechanism transition from a carrier trapping/detrapping type to an electrochemical-redox-reaction-controlled conductive filament formation/rupture process. The Auger electron spectroscopy (AES) results demonstrate that the Cu atoms changes to Cu^{2+} after RTA treatment. Once the Joule heat is involved, the switching properties may become polarity-independent and state can be switched to HRS by both positive and negative bias. Guan et al. [79], reported the nonpolar resistive switching phenomenon of the Cu/Cu:ZrO_2/Pt structure device and explained that the set process and reset process stem from the electrochemical reactions, and the localized Joule heating assisted oxidation reaction is involved during reset process. Cu/HfO_2:Cu/Pt reported by Wang et al. [80] also exhibited the nonpolar switching properties. The Cu ions electromigrate toward the cathode and are reduced to metallic Cu atoms. The electromigration reaction may not be the only dominant model since the Joule heating is included. Similar results are also observed on Cu/ZrO_2:Cu/Cu by Liu et al. [81] and Hg/$CuInO_2$/Cu_2O/CuO/Au by Varandani et al. [82].

Some groups use the metal organic materials, such as Cu-7,7’,8,8’-tetracyanoquinodimethane (CuTCNQ), as possible materials for data storage. In 1979, Potember et al. [83] first demonstrated the reproducible switching behaviors in memory structure of metal/CuTCNQ/Al stacked layers, and observed the endurance of 10^4 with high to low resistance ratio of about 100. In recent reports, this material attracts much attention due to its lower cost process and easy compatible with back-end of line (BEOL) interconnect process. The switching mechanism of CuTCNQ-based memory elements have shown that a combination of CuTCNQ and a dedicated “switching layer (SL)”, and RS is attributed to the formation and dissolution of Cu bridges through an interfacial oxide layer between CuTCNQ and SL, which the electroechemical reactions in the filament is involved. Muller et al. [84] have investigated the electrical performances of memory elements including a variety of SL, such as Al_2O_3, ZrO_2, HfO_2, or SiO_2. They further investigated the cross-section microstructure of CuTCNQ nanowires (NWs), which is formed by a solid-gas reaction between a sacrificial copper layer and TCNQ gas. Cross-sectional TEM images and SEM images are used to observe the microstructure shapes [85], and the conductive-AFM technique is used to detect the local switching [86].

As for the Ag electrode, it was mainly used for the Ag-based metal oxide, and solid electrolyte materials. Ag/$(AgI)_{0.5}(AgPO_3)_{0.5}$/Pt by Guo et al. [87], Ag/AgI/Pt by Liang et al. [88], Ag/Ag-Ge-S/W by Russo et al. [89], Ag/Ag_2S/Pt by Morales-Masis et al. [90], Ag/$(AgI)_{0.2}(Ag_2MoO_4)_{0.8}$ (AIMO)/Pt by Yan et al. [91], Ag/$Ag_{30}Ge_{17}Se_{53}$/Pt by Chen et al. [92], and Ag/$Ag_{30}S_2P_{14}O_{42}$ (ASP)/Pt by Guo et al. [93], all propose a similar model concerning the formation and rupture of Ag bridges by redox reactions, which suggested to account for the memory effect based on the metallic Ag bridges. Even, the transition metal oxide and perovskite oxide material can also be the solid electrolytes, such as Ag/ZnO:Mn/Pt by Yang et al. [94], Au/ZrO_2/Ag by Li et al. [95], and Ag/$SrTiO_3$/Pt by Yan et al. [96], indicating that the Ag^+ ions migrate through the STO film to accumulate a metallic Ag nanofilament and dissolve back under the opposite applied bias. Xu et al. [97] investigated the LCMO thin film by using Ag, Al and Al-50%Ag alloy metals as top electrode to control the Ag contents. The I-V sweeping current loop will highly depend on what electrode material is used as top electrode. Al-50%Ag/LCMO exhibits a counterclockwise current loop, while Al is clockwise one, which indicates the resistive switching mechanism changes from valence change type (we will discuss next paragraph) to conducting bridge type. Guo et al. [98] prepared Pt/Ag structures on SiO_2 substrates first, and then formed Pt/H_2O/Ag cells by adding de-ionized H_2O to the coplanar Pt/Ag structures. From the scanning electron microscopy investigations shown in Fig. 1-23, it clearly showed the growth and dissolution of Ag dendrites during resistive switching.

The solid electrolyte materials can been extensively investigated for their electrochemical application on solid-state. Among the electrolytes, Cu_2S and Ag_2S have attracted much attention due to their good ionic conductibility, and can be used to fabricate the Ag_2S nanowire. The nanowire shape can further scale down the cell size artificially. For Cu_2S material, Liu et al. [99] based on cation-deficient Cu_2S p-type semiconductor to fabricate the aligned Cu_2S nanowire for the RRAM application. The Cu_2S material can provide high mobility of Cu^+ vacancies in Cu_2S under applied bias, which may be a fast switch element for RS application. Liao et al. [100] synthesized the Ag_2S nanowires through a hydrothermal method with the reactants of $AgNO_3$, octadecylamine solvent, and sulfur powder. Pi et al. [101] used the self-made anodized aluminum oxide (AAO) and fabricated the Ag_2S nanowires by anodization process.

1.4.3 Bipolar switching mechanism – Valence Change System

Most of the binary transition metal oxides as well as complex composition oxides which exhibited the resistive switching characteristics belong to this category, even though the electrodes do not inject metal cations into the TMO films. This type of switch can easily be performed by applying the different polarity of bias on the devices, based on variation on the different valence states. Considering the matters to cause the different valence states, including injected electrons, oxygen ions, oxygen vacancies, and doping impurities, may modulate the distribution of the species inside TMO film and lead to different resistance values. In the following, we will introduce the valence change memory based on (i) trapping/detrapping of injected electrons at the M/O interface, (ii) trapping/detrapping of injected electrons at the bulk film, (iii) trapping/detrapping based on Mott transition, (iv) the intrinsic oxygen reservoir, (v) oxygen ions or vacancies migration (the extrinsic oxygen reservoir), and (vi) doping impurities, respectively.

This kinds of switching ((i), (ii), and (iii)) indicates that the RS mechanism is mainly based on the amounts of trapped electrons, i.e. the ratio between filled/unfilled to dominate high or low state. It’s hard to exactly divide this RS behavior because the injected electrons are always determined by the atomic composition ratio inside TMO films. Any change on the composition ratio, such as oxygen or metallic related defects and doping impurities, will alter the number of injected carriers. Therefore, for simplicity, we exclude the types of switching mechanism of migration of the defects, mobile metallic ions, oxygen ions, and related doping impurities that induces the alternation of the injected ions in this category, and only discussed the trapping/detrapping behavior at the interface or bulk side via the stable oxygen vacancies or metallic defects. We classify the trapping/detrapping of injected carriers into this type of switching because the valence change may be induced by the trapped charges, e.g. $Ti^{4+} + e^- \rightarrow Ti^{3+}$ or $Cu^{2+} + e^- \rightarrow Cu^+$ transition.

(i) The trapping/detrapping of the injected electrons can dominate the RS characteristics at the interface or at the bulk. In the beginning, we discuss the interface case first. Some of the groups suggested that the Schottky barrier at the M/O interface will regulate the injected carriers, like the Au/$LaTiO_{3+x}$/Sr(Ti,Nb)O_3 by Schmehl et al. [102], Ti/$Pr_{0.7}Ca_{0.3}MnO_3$/$SrRuO_3$ by Sawa et al. [103], and electrode/NiO/Pt by Seo et al. [35]. The following two reports, as $SrTiO_{3-\delta}$/Nb-doped $SrTiO_3$ by Ni et al. [104], and Pt/Nb-doped $SrTiO_3$/n^+-Si by Seong et al. [105], revealed that a large high-to-low resistance ratio is related to larger oxygen-related defects generated at the M/O interface, which can induce more interface traps at the interface, as shown in Fig. 1-24. Ouyang et al. [106] claimed that the electrode dependence of the resistive switching in Au/PS$^+$ Au-2 NT NPs/Al structure is attributed to the contact potential at the contact of gold nanoparticles and electrode arising from charge transfer between them. Yu et al. [107] investigated the structure effects on resistive switching of Al/TiO$_x$/Al devices and observed that only the area of the top electrode primarily takes part in resistive switching from the experimental results. This type of RS do not perform a forming process before operating the switching behavior, thus, the Schottky barrier formed between electrode and TMO film does not break. We suggest that therefore the injected carriers can be retained and confined at the interface and does not penetrate into TMO films.

(ii) The second, we introduce the trapping/detrapping of the RS behaviors at the bulk films. This type of switching is most observed on the Cu$_x$O thin film because the Cu$_x$O films are consists of cuprous oxide (Cu$_2$O) and cupric oxide (CuO). Cu$_2$O contains multiple levels of donor- and acceptor-type traps caused by copper and oxygen vacancies. The leakage current in Cu$_2$O film was reported to be related to the space-charge-limited conduction (SCLC) [108]. The SCLC conduction will follow the three specific steps: $I \alpha V$ correlation (Ohmic), followed by $I \alpha V^2$. After a dramatic increases on the current values, the current will obey the second $I \alpha V^2$ relation (Child's law) [109]. For the first part of the current, the ohmic behavior, the density of thermally generated free carriers inside the Cu$_x$O films is larger than the injected charge carriers. The ohmic conduction (J_{ohm}) is also named as trap-unfilled-limited conduction, and the equation in the ohmic conduction is $J_{ohm} = qn_0\mu_n \frac{V}{d_s}$, where q

and μ_n are the elementary charge and electron mobility in Cu_2O film. Once the injected carriers dominate the thermally generated carriers, the current conduction changes to $I \alpha V^2$ relation, thus this part of conduction is denoted as trap-filled-limited conduction (J_{TFL}). The transition voltage from the ohmic to trap-filled-limited behavior is defined as V_{on}, and the equation in the trap-filled-limited conduction can be $J_{TFL} = \frac{9}{8}\varepsilon\mu_n\theta\frac{V^2}{d_s^3} = \frac{9}{8}\varepsilon\mu_n\frac{V^2}{d_s^3}\left(\frac{N_c}{N_t}\right)e^{-\frac{E}{kT}}$, where ε is the dielectric constant and θ is the ratio of the free carrier density to the total carrier density. A relation between unfilled trap density and trap depth can also be described as θ-ratio. When all of the traps are filled with the injected carriers under the higher voltage, a sudden jump in current occurs at V_{TFL} and then the I-V behavior follows Child's law (J_{Child}), and the equation is $J_{Child} = \frac{9}{8}\varepsilon\mu_n\frac{V^2}{d_s^3}$. Therefore, once the conduction behavior belongs to SCLC current, trapping/detrapping is the most used to elucidate the switching characteristics, as the Pt/Cu_xO/TiN structure reported by Yang et al. [110]. Since the SCLC current is mainly dominated the trapped carriers and trap state numbers, a further discussion on the trap depth and temperature related to the conducting current is investigated [111]. Based on a quantitative thermal detrapping analysis, the retention time can be determined from the trap depth and given temperature, as shown in the equation: $\frac{1}{kT_c} = \frac{\ln\left(t/\tau_0\right)}{E} + \frac{1}{0.0259\ eV}$, where t is the measurement time, τ_0 the RT retention, and E the trap depth, and T_c is the temperature where retention of the memory cells is reduced to the measurement time t. The erasing characteristics of Cu_2O are power-driven process, which are related to the thermal effect of power dissipation [20]. Within the proposed switching model based on charge trapping, erasing can be explained by field assisted thermal emission of trapped charges. Tsai et al. [112] investigated the electrical conduction behaviors of the SiO_x films and observed that the existence of the RS is highly correlated to the conduction behavior, as related to different amount of traps inside SiO_x film. Trapped electrons moving inside the SiO_x thin film under applied bias result in modulation of the band bending, and the amount of traps would influence the bias voltages of switching resistance state and the retention time. Even the copolymer material reported by Hong et al. [113] was also explained its resistive switching behaviors by trap charging and discharging.

Some of the TMO films can also be induced defects or vacancies inside the bulk film by doping impurity or implanted other species. Lee et al. [114] investigated the resistance switching of Pt/nonstoichiometric Zr:NiO_x/p^+-Si sandwich structure. They proposed that the switching mechanism can be explained by electron trapping and detrapping through the excess Zr^+ ions in TMO layer. Similar results are also observed on Au/Cr/Zr^+-implanted-ZrO_2/n^+-Si by Liu et al. [115,116]. The embedded metal-nanoparticles inside TMO film can also induce the trapping/detrapping properties. Guan et al. [117] intentionally introduced Au nanocrystals in ZrO_2 films and observed that the device yield can be improved since the embedded nanocrystals can improve the trap concentration. The oxygen vacancies existed inside the TMO films can also provide for the injected carriers trapping/detrapping under applied bias. Xia et al. investigated the complex impedance spectroscopy of $(Ba,Sr)(Zr,Ti)O_3$ thin films in the HRS and LRS for RRAM applications. From the notation defined by Kroger and Vink, the oxygen vacancies lead to shallow level electrons, which may be trapped by Ti^{4+} ions or oxygen vacancies and are easy to be activated becoming conducting electrons. Jeong et al. [118] used the organic material – poly(3,4-ethylenedioxythiophene):polystyrenesulfonate (PEDOT:PSS) thin films as memory thin films sandwiched between Al electrodes. The bulk positive space charges induced by the segregation of PSS^- chains is the dominant role in electron charge trapping/detrapping process of SCLC conduction system.

(iii) The third part of the trapping/detrapping mechanism is based on Mott transition, which a three domains model may be used to support this elucidation. For a metal-insulator-metal sandwiched structure, Rozenberg et al. [119] proposed a model with just three types of domain, schematically depicted in Fig. 1-25. The top and bottom are assumed to be smaller than the middle one, and the differentiation might be justified by the different electronic states near the M/O interface. This model provides a useful guidance for the understanding of the switching properties. They further constructed a model based on domains concept in 2007 including the strong correlation effects [120]. A large domain in the bulk behaves as a charge reservoir, and the domains at the metal/oxide interface regulate the current as barriers. Under the applied bias, the injected electrons accumulated near the electrode are strongly correlated and trigger the Mott transition. This model is mainly used to explain the strong correlated perovskites such as the doping-induced insulator to metal transition and the spatical inhomogeneity. The Au/PCMO/Pt by Kim et al. [121,122], and Ag/PCMO/Pt by Fujimoto et al. [123] based on Mott transition model to explain their switching characteristics. A high-speed resistive change of the Pt/TiO_2/Tin structure was derived from the Mott transition by Fujimoto et al. [124].

(iv) This category collects the MIM structures using the natural oxygen reservoir material as top electrode, such as TiN, indium tin oxide (ITO), indium zinc oxide (IZO), etc. The role of oxygen reservoir can effectively restore the attracted oxygen ions under the applied bias and then repel back into the TMO films at next operation with the opposite bias, which a positive bias applied on TiN electrode for SET process and a negative one for RESET process is necessary. Therefore, this kind of RS is dependent on where the TiN material as electrode. Several groups have reported that the TiN can be a good oxygen reservoir material to perform the RS characteristics, including TiN/ZnO/Pt by Xu et al. [125], TiN/ZrO_2/Pt by Sun et al. [126,127], TiN/TiO_2/Pt or Pt/TiO_2/TiN by Do et al. [128], and Pt(or Ti)/InGaZnO/TiN by Chen et al. [129]. Although whether the TiN material as top or bottom electrode can both perform the switching characteristics, there is a little difference between the two structure of metal/TMO/TiN and TiN/TMO/metal device. Kwak et al. [130] investigated the TiN/TiO_2/TiN stacked structure and observed the nature of an interfacial layer TiO_xN_{1-x} formation between the TiO_2 and TiN bottom electrode by inter-diffusion process of oxygen and nitrogen atoms during the deposition of the TiO_2 insulator layer. The thin interfacial TiO_xN_{1-x} layer might play a role as a diffusion barrier to mobile oxygen ions, and yields the difference in the current levels of different electroforming polarities.

(v) This kind of resistance switching based on the difference of amounts of oxygen ions, oxygen vacancies, or oxygen-related defects inside the insulator film, which are related to the migration effect of the oxygen ions and vacancies triggered by the applied bias. Lin et al. [131] proposed the specific viewpoint first by utilizing the reactive metal Ti, which with the oxygen getter character, to influence the oxygen ions and vacancies distribution in the vicinity of TMO films. Owing to interdiffusion between Ti and TMO film, an interfacial layer is formed between the electrode and TMO. This will induce oxygen vacancies at the top part of the TMO film, and the IL can serve as a series resistance and oxygen sink. The similar phenomenon can both be observed on ZrO_2 [132,133], and Al_2O_3 [134] materials. After this series of investigation, the researchers observed that the oxygen-related defects can also be modulated from the external fabrication process and post treatment, such as top electrode, inserting metal thin layer in TMO film, stacked structures, and post treatment under H_2, O_2/Ar, or high temperature circumstance, etc. Once the atomic composition and distribution are altered by the external process, the RS may differ. Therefore, a deep discussion on how the different electrode metal and fabrication process influence the switching behaviors will be totally discussed in the next following section 1.4.2.

(vi) By doping impurities, the TMO thin film can also be modified to different valence states inside the insulator films. Lin et al. [135] reported the V-doped $SrZrO_3$ thin films and investigated its resistive switching properties. The V doping effect is achieved by Zr^{4+} sites being substituted by V^{5+} ions, which results in suppression of the formation of oxygen vacancies. Lin et al. [136] takes the site, mass, and charge balances into account and reported the possible defect equations. They explained that not only the oxygen vacancy concentration is reduced with vanadium doping but also the electron concentration is increased. Zhang et al. [137] calculated the behaviors of oxygen vacancy, including defect energy level and formation energy, on metal (Al, Ti, or La) doped ZrO_2 by first principles calculation. The calculated results reveal that dopant chemical valence has significant impact on oxygen vacancy behaviors.

1.4.4 Influence factors to the bipolar resistive switching

This section is like section 1.3.2 that a variety of factors will influence the switching properties. The switching mechanism of the bipolar resistive switching is much complicated than that of unipolar one, therefore, a little change on the microstructure and composition may dominate the switching properties to different switching mechanism, as we discussed above the bi-switching mechanism. The basic stacked structure M-I-M has been investigated in detail to find out the relationship between each two parameters. A similar description like unipolar one will be discussed in the following steps: the buffer layer or metal thin layer, which inserted at the top electrode (TE)/insulator, at the middle insulator, or at the insulator/bottom electrode (BE), stacked structure, doping impurities with additional atoms by implanted or annealing, embedded metal nanoparticles inside TMO film, and special structure like nanowires or nanorods, have been demonstrated. A correlation between this influence factors and valence change memory will be linked.

(a) Electrode

We have reported above that the metal thin film has its specific work-function (WF), electron affinity, and Gibbs free energy for oxygen, as well as the different contact properties when in contact to different insulator films. Since the interaction may occur at the interface, the resistive switching characteristics can be greatly influenced and determined by the properties of this IL. So, we may discuss the electrode effect first and then the separate them into different categories.

(i) Schottky barrier modulation

The effect of the Schottky barrier formed between the metal/insulator is regard as one of the critical factors on switching properties. The Schottky barrier can influence the conducting current by regulating the injected carriers into the TMO thin films. Schottky barrier height modulation by trapping and detrapping the injected carriers are discussed as shown in last section. Here, some groups based on the migrated oxygen ions and vacancies to generate a plausible model for the Schottky junction modulation. Choi et al. [138] reported on Pt/$PbZr_{0.3}Ti_{0.7}O_3$/LSCO structure that the contact potential decreases as the positive bias was applied on Pt electrode, and the generated oxygen vacancies can form tunneling paths for electron conduction. By applying a negative bias on the Pt top electrode, large amounts of oxygen are accumulated in oxygen vacancies, thus preventing electrons tunneling. Similar explanation was also proposed by Pt/$SrTiO_3$ by Kim et al. [139]. Lee et al. [140] observed the NiO film by using a scanning probe as the top electrode. The modulation of the potential barrier width and resulting tunneling current through the interface may be attributed to accumulation/depletion of injected holes or oxygen vacancies caused by the electrochemical reaction.

Shang et al. [141] studied the Schottky junction of Au/$SrTiO_3$ structure by using photovoltaic effects under different applied electric pulses. They observed the corresponding Schottky barrier, which was deduced from the photoresponse data about 1.5 eV, is independent of junction resistance. The observed results reveal the invariance of the interfacial Schottky barrier during resistance switching. We suggested that the resistive switching may occur at the localized region, therefore, the macroscopic investigation of photovoltaic analysis may detect insensitively.

(ii) Gibbs free energy

We have previously reported that the effects of electrodes on the unipolar switching properties must be considered as a critical factor in pursuit of the appropriate metal materials as electrodes [37]. For the bipolar operation, the analysis of the bipolar I-V curves strongly depend on the Gibbs free energy of oxidation of the TEs are investigated on PCMO thin film by Liao et al. [142]. From the measurement of virgin resistance (VR, i.e. the contact resistance) between the TE and PCMO film, the observations suggest that the interface is not a typical Schottky barrier formed at the interface, but is somehow associated with the presence of the interfacial metal oxide. The VR information, I-V curves, and its related microstructure are shown in Fig. 1-26 and Fig. 1-27. The metal/PCMO/Pt devices can be categorized into two groups, which based on the Gibbs free energy for oxidation of the TE is larger or less than PCMO oxidation free energy. When nonreactive metal group (Pt, Ag, Au or Cu) was used as electrodes, no RS properties are observed, while the RS properties occurs with forming-free character when reactive metal is used as top electrode. The reactive metal with lower free energy for oxidation than PCMO film can easily induce an interfacial metal oxide at the interface and modulate the oxygen vacancy concentrations in the vicinity of insulator film. Under the applied positive bias, the oxygen ions migrated from the PCMO film to the reactive metal and oxidize with reactive metal to form a thicker interfacial layer, thus the resistance state switched to HRS. As the negative bias was applied, the dissociation of the metal oxide layer by the redox reaction at the metal/PCMO interface. Li et al. [143,144] reported the similar concepts to explain the free energy effect on switching properties of PCMO films. Shono et al. [145] and Kawano et al. [146] further observed the microstructure change of the interfacial metal oxide by cross-section TEM investigation under the applied bias. Yang et al. [147] investigated the switching behaviors of M/LCMO/Pt junctions and found that the switching polarity of the junctions for M=Pt, Ag, and Cu was opposite to those for M=Al, Ti, and W based on Gibbs free energy for oxidation. A little difference from the PCMO film [142] is that the opposite switching direction can be observed on the metal whose free energy is larger than LCMO film. Though the low free energy for oxidation metals can attract oxygen ions easily during the interfacial metal oxide formation, but the reduction of their oxides require more power and longer switch time since the formation and dissociation of the interface oxide determine the switching speed. Hasan et al. [148] improved the switching speed of LCMO/Pt films by substituting the less reactive metal Al for the Sm metal. Liu et al. [149] used the less reactive metal W as electrode and obtained a low power reset switch of only a maximum current of about 4 μA, which is much lower than the

Al/PCMO/$LaNiO_3$ structure by Harada et al. [150] and Al/PCMO/Pt by Jo et al. [151].

Although the reactive metal can easily modulate the distribution of the oxygen contents and vacancies inside the TMO film and results in RS behaviors, the switching mechanism does not all the same. As we followed the description above [142], Al/TiO_2/Al by Jeong et al. [152,153], Al/PCMO/Pt by Seong et al. [154], and Ti/PCMO/Pt by Liu et al. [155] reported that the reactive metal can form an interfacial metal oxide at the TE/TMO interface, and the switching mechanism is dominated by this metal oxide layer under applied bias. The I-V sweeping curves exhibit the clockwise loop in semi-logarithm plot. However, an opposite sweeping curves, i.e. the counter-clockwise loop, was observed when the reactive metal contacts on the following oxide film, such as CeO_x, Cu_xO, HfO_2, ZrO_2, and Al_2O_3 films. There are several explanations on their respective material, including (i) external oxygen reservoir, (ii) oxygen vacancy-riched layer. This is why they are categorized into the valence change memory, because a stacked structure composed of different oxygen contents will be formed. The stacked oxide structure can provide defects, traps, or space for the oxygen ions or vacancies migration under the applied bias, thus the switching behaviors can be obtained. (i) The external oxygen reservoir is used to differentiate from intrinsic oxygen reservoir TiN because this kind of reservoir is attributed to the formation of the interfacial metal oxide. Ti/ZrO_2/Pt by Lee et al. [156,157,131,132,133], and Al/Al_2O_3/Pt by Wu et al. [158,134] based on this concept and explained that this metal oxide can change the switching from unipolar (noble metal) to bipolar operation. Oxygen ions diffuse in and out of the interfacial metal oxide is used to explain their switching mechanism. The switching involves the thermal Joule heat may also observed in Al/Cu_xO/Cu structure by Lv et al. [159]. (ii) The reactive metal will induce an oxygen vacancy-riched layer, as reported by Al/CeO_x/Pt by Sun et al. [160]. The switching properties are dominated by aligning or breaking the filamentary paths composing of oxygen vacancy both inside the vacancy-riched layer and vacancy-deficient layer. Although both the Al and Ti are reactive metals and can oxidize by attracting oxygen ions from the below layer, the characters between them is not totally the same. Because of the self-stop oxidation nature character of AlO_x, the Al metal layer is more suitable as an oxygen reservoir than that of Ti metal one. The Ti metal can easily over-extract the oxygen ions from the underlying TMO films, thus causing the RS failure easily [159]. This problem can be ameliorated in the following section – by controlling the Ti thickness.

(b) Metal thin layer inserted at M/O interface

Lee et al. [161] compared the switching characteristics of $AlCu/HfO_2/TiN$ structure with and without the inserting layer TiN/Ti at the $AlCu/HfO_2$ interface. They suggest that the Ti metal can induce more oxygen vacancies as the trapping centers than that of AlCu electrode does in the HfO_x layer. By well controlling the Ti effect, a forming-free device [162] and high yield device [163] can be achieved. However, some authors may regard the Ti as TiO_x metal oxide during fabrication because of its oxygen getter nature, as we discussed last section.

(c) The buffer layer inserted at M/O interface (stacked structure)

Because the switching characteristics can be easily modulated by the electrode based on the model we summarized, some groups modifies the switching properties by inserting the buffer layer or metal thin layer at the M/O interface. The purpose of the additional process is for the improvement of the switching behaviors, as well as the switching parameters dispersion. Chen et al. [164] reported that the stacked $TaN/Al_2O_3/NbAlO/Al_2O_3/Pt$ structure exhibits better uniformity than TaN/NbAlO/Pt device. The inserted layer can induce the similar effect like we discussed above: an external oxygen reservoir (Pt/Cr:SZO/TiON/Pt reported by Park et al. [165]). The oxygen vacancy-deficient/vacancy-riched stacked structure was deliberately fabricated and oxygen ions or vacancies can be triggered by the applied bias, causing the formation and rupture of filaments at the interface of the stacked structure, as Pt/TiO_2/TiO_{2-x}/Pt by Do et al. [166], Pt/ZrO_x/HfO_x/TiN by Lee et al. [167], Ti/TiO_x/LCMO/Pt by Liu et al. [168], Pt/Ta_2O_5/TaO_x/Pt by Hur et al. [169], and Al/SZO(OR)/SZO(OD)/LNO/Pt by Lin et al. [170]. When the top portion of the stacked oxide layer is quite thin (TiO_x in [168] and Ta_2O_5 in [169]), the authors suggest that the whole top portion oxide takes part in the resistive switching, i.e. the formation and dissolution of filaments occurs at the top portion oxide layer.

(d) Metal thin layer inserted in the middle of insulator film

Inserting a metal layer within the oxide layer followed by post annealing is another beneficial way to improve the switching stability. The inserted metal layer can induce many defects inside TMO thin film and produce a space charge region for oxygen ions migration, as reported in the Al/SZO/Cr/SZO/LNO structure by Lin et al. [171], Ti/ZrO_2/Mo/ZrO_2/Pt by Wang et al. [157], and TiN/HfO_2:Al layer/Pt by Yu et al. [172].

(e) Embedded metal nanocrystal (NC)

The embedded metal NCs are reduced from the metal thin layer under high temperature post annealing process. This additional NCs can provide the benefits of improving the fluctuation of switching parameters, which may be attributed to the local enhancement or concentration in electric field induced by the embedded NCs. The structures of Au/ZrO_2:nc-Au/n^+-Si by Zuo et al. [173], Pt/TiO_2:nc-Pt/Pt by Chang et al. [174], and Al/$SrZrO_3$:E-Pt/Pt by Lin et al. [175] all observed an improvement on their switching characteristics. Reduction on the effective oxide thickness may also strengthen the electric field on some localized spots points.

(f) Post annealing

Post annealing can modulate the thin film morphology, surface roughness, crystallinity, electrical characteristics, atomic composition and binding energy, and the resistive switching properties. The treatment process is performed to improve the resistive switching stability. Au/PCMO/Pt by Kim et al. [118,119], Pt/Ti/Al_2O_3/Pt by Lin et al. [176], Pt/TiO_2/Pt by Kim et al. [177], and Cu/BFO/Pt by Yin et al. [178] observed that the crystallinity of TMO thin film increases with the annealing temperature increasing. Since crystallinity increases, then the grain size increases [178], followed by the reduction on root mean square [177] and operation voltage [176,178]. Yang et al. [179] observed the opposite properties that the grain size of Cu_2S thin film in Cu/Cu_2S/Pt structure decreases with increasing annealing temperature. However, they all have a larger high to low resistance ratio after annealing. Liu et al. [180] reported an opposite result because oxygen annealing can lead to the decrease of oxygen vacancies in the LCMO surface, thus causing the ratio decreasing.

1.4.5 Improving switching stability

As we mentioned above, there are plenty of switching mechanism for explanation on the bipolar switching properties. Therefore, different switching types of RRAM may need the specific technique to improve the stability. To perform a stable M-I-M structure, one can roughly separately into three main goals: one is the main insulator bulk thin film (single or stacked), and the second is the suitable metal top and bottom electrode (reactive metal, noble metal, or compound metal), and the last one is the additional process to modulate the final switching properties (post-thermal anneal, plasma treatment). Among the reported data, we summarized the methods to reduce switching parameters dispersion of bipolar RS characteristics as follows: (a) electrode, (b) embedded metal layer, (c) buffer layer, (d) operation modulation, and (e) TMO film treatment.

(a) Electrode

Feng et al. [181] used compound $Fe_{0.73}Pt_{0.27}$ metal instead of pure Fe metal as the bottom electrode of TiN/SiO_2/BE thin film to improve the switching stability. The improvement is associated with the decrease in the Fe content in the FeO_x layer.

(b) embedded metal layer

As we have mentioned above that the embedded metal layer inserted inside the TMO thin film can induce many defects inside TMO thin film, produce a space charge region for oxygen ions migration, and reduce the effective TMO thickness. Some reports were done in the following references [157,171,172].

(c) buffer layer

The stacked oxide layer can provide the benefit of confining the filament formation and rupture at some localized region at the interface, as reported in reference [164] and [168].

(d) operation modulation

Since the resistance values of RRAM devices are easily triggered under the applied bias, this improvement is based on the improvement of the operation skill. Yin et al. [64] changed the pulse operation from single square pulse to ramped-pulse series

(RPS) to avoid the RESET instability and minimize the V_{reset} dispersion. Biju et al. [182] improved the switching characteristics of TiO_2 films by well choosing a proper compliance current in the first set operation. The gradual reset process, which is due to the multiple filaments rupture in a random manner, can be reduced by setting a higher compliance current in the first operation. Leaving sample leaky paths in HRS shows significantly improvement on switching uniformity of Cu/CuC/Pt, was reported by Park et al. [183].

(e) Treatment

The electrical characteristics of RRAM can be modulated via TMO surface treatment. Cho et al. [184] reported that samples undergone additional plasma treatment exhibits the larger resistance values and on/off ratio. Lin et al. [170] modulated the $SrZrO_3$ memory devices layer to oxygen-rich and oxygen-deficient stacked layers. The stacked layer can confine the rupture spots at some localized point at the interface, as we discussed previously. Therefore, the switching dispersion can be reduced.

1.5 Forming process

The forming process is the operation to induce oxygen-related or metallic defects inside the TMO thin film under the applied bias to certain voltage value (to an abrupt jump on conducting current is needed), thus causing filamentary conducting paths inside TMO for conduction. After the electroforming process, then the reproducible and reversible resistance switching characteristics can be performed by current or voltage applied bias. This forming operation is like breakdown test, however, a current compliance is sometimes needed to protect the device from totally hard breakdown. Some groups called them as ‘soft-breakdown (SBD)’. Forming can be demonstrated in a variety of types, includes thermal forming, and electroforming. Even the time to breakdown (TDDB) was adopted to perform the switching characteristics [25,185].

1.5.1 Early forming model

From 1960's, the forming process has been discussed and several possible models have been proposed to explain the electrical behavior. Hickmott et al. [15,186] proposed the forming model is Schottky ionization of impurities near middle of bandgap, which forms the localized states and space charges for the electrons injection. Simmons and Verderber et al. [16] suggested that the injection of ions from anode will form a broad impurity band inside the midgap. The injected ions may form space charge and cause band bending. Dearnaley et al. [187] proposed that the forming process is a local propagation of conducting filament through insulator film. The forming begins at anode and can be stopped when the released oxygen gas react with anode film. Greene et al. [188] claimed the oxygen causes competing reaction at cathode and the injection of vacancies from cathode would be obtained under high-field bias.

1.5.2 Detail forming phenomenon

In the case of oxides, the electroforming process under the electrical stress can be explained by the creation and redistribution of oxygen vacancies inside the TMO films. Alternation in the oxygen vacancy concentration leads to changes in the conductivity, and the filamentlike defect structures inside the insulator film thus determining the thin film conductivity. The electrochemical reaction of oxygen vacancy and gas formation at the anode can be expressed in the Kroger-Vink notation as $O_O^X \rightarrow V_O^{2+} + 2e^- + \frac{1}{2}O_2$. The evidence of removing oxygen ions from the crystal lattice during the electroforming process is the appearance of gas bubbles, as reported by Szot et al. [189], Jeong et al. [190], and Yang et al. [191]. The deformation of the microstructure owing to the bubbles gas is shown in Fig. 1-28. The detail electroforming process can be depicted as follows. Oxygen vacancies are formed first at the TE/TMO when positive bias was applied to the TE, leading to the reduction of the SBH at the TE/TMO interface (followed by the Kroger-Vink notation). The TE/TMO interface can serve as a source of oxygen vacancies as Pt/TiO_2/Pt by Jeong et al. [190,192], Au/TiO_2/Pt by Yarmarkin et al. [193], Pt/STO(Fe)/Nb:STO by Menke et al. [194], and Pt/STO/Pt by Yan et al. [195] reported. Jeong et al. [190] reported a detail description about forming that the oxygen vacancies (Vo^{2+}) will migrate to the BE by drift or diffusion to the electric field, thus causing a gradient of the oxygen vacancy concentration. The migrated oxygen vacancies accumulate at the TMO/BE interface, and then the conduction path grows toward TE continuously. Similar explanation are reported by Menke et al. [194] and Yan et al. [195], but a different forming model is constructed based on the impedance measurement. Some forming effect, like the current or voltage bias forming [196] and thermal or electrical forming [197], is also discussed. They all conclude that the forming process occurs in a localized spot electrochemically, and the microstructural morphology changes are further confirmed by the spatially-resolved near-edge x-ray absorption fine structure (NEXAFS) spectroscopy. [198]

1.6 Amorphous RRAM

Generally, most of the materials reported above are polycrystalline structures, and the existence of the grain boundaries may facilitate the formation of the conducting filaments and determine its electrical properties. In recent years, amorphous material attracts much attention because of its characteristics of free from grain boundaries, which can improve films uniformity and avoid the detrimental pad-to-pad variations in switching characteristics due to diverse grain boundary nature of the polycrystalline cells. The numbers of published papers before 2010 based on the amorphous thin film are few, but more than ten papers are proposed in 2010.

1.6.1 Unipolar switching

The unipolar switching characteristics of the amorphous thin film are also mainly based on the electric-field driven for SET and thermal Joule heat for RESET process. Spiga et al. [36] compared the electrical properties of poly NiO and amorphous Nb_2O_5 film and concluded that Nb_2O_5 can provide better film uniformity and easy process control. Gao et al. [199] proposed the Lu_2O_3-based RRAM devices and explained the possible mechanism might be attributed to redistribution of oxygen vacancies along filamentary paths. Chen et al. [200] compared the switching behaviors of Ti doped SiO_x film when different metal was used as top electrode. Li et al. [201] observed that the transition between high and low resistance state of $LaLuO_3$ film is attributed to the change in the separation between oxygen vacancy sites, which is discussed based on the concept of correlated barrier hopping (CBH) theory.

1.6.2 Bipolar switching

For bipolar RRAM, the switching mechanism can also be divided following the categories we summarized above. Cu/CuC/Pt by Pyun et al. [202], HfO_2/CuTCNQ/Pt by Muller et al. [86], Cu/a-C:H/Pt by Zhuge et al. [69], Pt/a-TiO_2/Ag by Busani et al. [203], and Ag/a-$Ag_{30}Ge_{17}Se_{53}$/Pt by Chen et al. [204] reported the switching properties are belonged to the electrochemical metallization, which the formation and dissolution of a conducting Cu or Ag metallic bridge under applied bias dominate the RS. Seo et al. [205] reported the Al/a-Si/Al switching behaviors is owing to the incorporation of the top metal migrated or diffused into a-Si layer. The following samples belong to valence change memory, which the switching mechanism is based on redistribution of the oxygen vacancies, includes structures of Pt/GaOx/ITO by Gao et al. [206], Al/a-TiO_2/Al by Jeong et al. [207], Al/a-TiO_2/ITO by Jung et al. [208], and anodic porous alumina (APA) by Oyoshi et al. [209,210].

1.7 Nonpolar switching

When a TMO can be performed both unipolar and bipolar resistive switching properties, then it was called nonpolar or polarity-independent switching. Compared between the unipolar and bipolar RS we summarized above, we have known the effect on the switching properties and its related switching mechanism. The basic unipolar switching is based on the electric-driven for SET and thermal Joule heating for RESET, but for the bipolar switching, the RESET can not only by the opposite electric-driven but also by the Joule heating. Therefore, atomic redistribution suffers competition between electric field bias or thermal heat accumulation during bipolar RESET process.

1.7.1 symmetric character

If the MIM stacked structure is near fully symmetric, i.e. the same contact resistance, interface barrier height or width, electrode metal characteristics, and uniform atomic and defect composition inside TMO thin film, then the nonpolar properties can be performed and the conducting behaviors between uni- and bipolar will be similar (operated at the same current compliance), all dominated by Joule heating for RESET process, as reported Pt/MgO/Pt by Huang et al [211], Au/ZnO/SS by et al. [212] and Ni/Cu_xO/Cu by Liu et al. [213]. Cu/Cu:SiO_2/W by Schindler et al. [214], Pt/TiO_2/Pt Jeong et al. [215], Pt/TiO_2/Pt by Schroeder et al. [190], Ag/ZnO/Pt by Lee et al. [216] reported that the different current compliance value during the electroforming process is needed to separate the switching behaviors between BRS and URS, and larger current compliance is needed for the URS. This implies under the same operation condition, the Joule heat can not be induced on their samples [213-216].

1.7.2 Asymmetric character

Some groups investigated the nonpolar behaviors on the specific oxide material based on the topic of oxide and electrode. As for the electrode effect, Lin et al. [131-133,217 ,218], Kim et la. [219], Do et al. [220], Wu et al. [158], and Zhang et al. [221] all reported that when one side of the electrode was changed from noble to reactive metal, such as Al or Ti, then the switching behaviors will change from uni- to bi-polar characteristics. We can link the electrode effect to uni- (in section 1.3.2 (b)) and bipolar (in section 1.4.4 (a)) electrical characteristics and conclude that the interface between anode/TMO is a critical issue for the RS behavior. We can observe that once the as-grown well-defined interface character is altered by the reactive metal, then the operation changes from uni- to bipolar, as can be related to the formation of an additional interfacial metal oxide at M/O interface. The additional layer deteriorates the TMO surface and induces an oxygen vacancy-riched region at the M/O interface. The oxygen vacancy-riched region is too leaky to trigger Joule heating occurs, therefore, the unipolar RS will lose its electrical behaviors. However, the oxygen vacancy-riched region is beneficial for bipolar RS. Different approaches may be needed when improving each switching characteristics.

1.8 Conduction behavior

RRAM has different resistance states which may be related to different specific conduction behaviors.

1.8.1 Ohmic Conduction

The Ohmic conduction results from thermally excited electrons to transform from one isolated state into the next state. The schematic diagram is shown in Fig. 1-29(a). If carriers transport in a nonconductor is by this mechanism, then the plots of $ln (J)$ versus $ln (V)$ at a fixed temperature will be a straight line with a slope of about 1. The relation between $ln (J)$ versus $1/T$ in a specific voltage will follow a straight line. The equation in the ohmic conduction is

$$J_{ohm} = qn_0 \mu_n \frac{V}{d_s} \tag{1-1}$$

where q and μ_n are the elementary charge and electron mobility.

1.8.2 Schottky Emission

The Schottky emission is caused by thermionic emission of electrons, as shown in Fig. 1-29(b). If carriers transport by this mechanism, a plot of $ln (J/T^2)$ versus $1/T$ in a specific voltage is a straight line, and $ln (J)$ versus $V^{1/2}$ at a fixed temperature is also a straight line. The I-V relation can be expressed as follows:

$$\ln\left(\frac{J}{T^2}\right) = \frac{-q\Phi_b + q\sqrt{\left(qE \big/ 4\pi\varepsilon_o\varepsilon_r\right)}}{kT} + \ln A^* \tag{1-2}$$

where J is the current density, e is the electronic charge, ε_o is the permittivity of free space, ε_i is the optical dielectric constant, V is the applied voltage, d is the thickness of a film, k is the Boltzmann’s constant, and T is temperature.

1.8.3 Poole-Frenkel Emission

The Poole-Frenkel emission is due to field-enhance thermal excitation of trapped electrons into the conduction band, as shown in Fig. 1-29(c). The plot of the P-F emission in ln (J) versus 1/T in a specific voltage and ln (J/V^2) versus $V^{1/2}$ at a fixed temperature are straight lines. And the P-F emission is highly relative to the trap density of the insulator. The current density and the electric filed (J-E) characteristics follow the relationship:

$$\ln\left(\frac{J}{E}\right) = \frac{-q\Phi_t + q\sqrt{\left(qE \middle/ \pi\varepsilon_o\varepsilon_r \right)}}{kT} + \ln A^* \qquad (1\text{-}3)$$

where E is the electric field, e is the electronic charge, ε_o is the dielectric constant of free space, ε_i is the high-frequency dielectric constant, k is the Boltzmann's constant, and T is temperature, and ϕ_t is the trap energy level with respect to the conduction band.

1.8.4 Fowler-Nordheim Tunneling

Tunneling is defined as a quantum-mechanism process in which a particle can pass through a classically forbidden region, as shown in Fig. 1-29(d). Considering the conducting current, tunneling is a process that allows electrons to pass from the energy levels of metal or semiconductor material to the other side through the intervening barrier of insulator film. The equation of Fowler-Nordheim tunneling current is given by:

$$J = \frac{q^3E^2}{8\pi h\Phi_b}\exp\left[\frac{-4(2m)^{1/2}\Phi_b^{3/2}}{3h' qE}\right] \qquad (1\text{-}4)$$

Where h is Plank's constant ($h'=h/2\pi$), Φ_b is injection barrier height, q is a single electron charge, m is mass of a free electron, m^* is effective mass of an electron in the bandgap of insulator oxide.

1.8.5 Space Charge Limited Current (SCLC)

The conduction mechanism indicates when charge carriers have been emitted from some region of a solid, and the carriers can form a space charge region. SCLC usually only occurs in Ohmic contact, lower injecting barrier, and lower mobility. Therefore, the charge tends to be rapidly repulsive. SCLC is direct proportion to V^2, and is essentially independent on the temperature. The detail equation has been listed in section 1.4.3 (ii).

1.9 Integrated RRAM & Array structure

(a) Crossbar array

One of the most promising applications with high density memory cells is the cross-bar type array memory devices, which is ideal smallest memory cell area of $4F^2$, where F is the minimum feature size. For an array structure, writing can be operated on each individual cell by selecting the two crossing lines and applied the appropriate SET or RESET bias to trigger the device. Other cells in the neighboring connected to only one of the two crossing lines will not be influenced because each line is connected to a lower voltage value than that of SET and RESET voltages. An array structures composed of 32×32 on CuC film by Pyun et al. [202] and 32×32 on Pt/SOG/Ag by Meier et al. [222-224] were published. The UV nanoimprint lithographt process is a beneficial technique for planarization, especially, it provides nanometer resolution, high throughput and low cost prospects. This technique can be adopted to fabricate the 3D stacked array structure, as shown on amorphous methyl-silsesquioxane (MSQ) by Kugeler et al. [225]. The three layer stacked crossbar organic memory arrays is fabricated by Song et al. [226]. The crossbar array device with a multi stack structure may offer the highest density of memory devices, which can be used in solid state disc-type devices. In addition, the structure is better suited for the defect-tolerant architecture which requires an extremely high density memory. Therefore, the crossbar array can be fabricated in an extremely high density structure but less demanding endurance requirements.

(b) 1T1R structure

However, when reading from a certain HRS cell, it can be seriously disturbed by other parallel connected LRS cells owing to interference effect. These issues can be addressed by adding the proper selection devices, such as the diode [227-229] or the transistor [230].

1.10 Conclusion

Although the basic RRAM device - MIM sandwiched structure is quite simple and easy fabricated, the RS characteristics are highly correlated to each thin film properties. Until now, thanks to various groups pay high attention on the unknown of the resistive switching behavior, the frame of the switching mechanism emerges clearly. We summarized the proposed effect, such as TMO composition, electrode material, post treatment condition, and etc., on the electrical characteristics of both unipolar and bipolar switching behaviors in detail. Switching mechanism of the RRAM can be broadly categorized into thermal Joule heat type, electrochemical metallization, valence change type, and bi-model. Based on the structures of the switching mechanism, several techniques are proposed to improve the switching stability. According to the paper reviews on nonpolar RS, we observed that the process window for unipolar operation is much smaller than that of bipolar one. From the viewpoint of heating temperature, a large conducting current is needed to induce high thermal temperature (current compliance needs large enough) while a too large conducting current (induced by reactive metal) will destroy the thin film property. From the viewpoint of material choice, a material that can tolerate high temperature near 1000 °C and easily be triggered under applied bias is needed. For a realization for next generation NVM application, 3D stacking crossbar array of memory devices provides a way to achieve high memory cells density. Incorporating a diode in series with each memory cells, the crosstalk and interference during reading each single cell can be effectively avoided.

1.11 Dissertation organization

Chapter 1 summarizes the introduction about novel NVM, resistive switching concepts of RRAM, and its related unipolar and bipolar switching mechanism. Several effects to the switching characteristics, improvement methods, nonpolar properties, and integrated stacked structure are also mentioned. Finally, we provide the motivation of the whole experimental investigation.

Chapter 2 first introduces the basic concept of the fabrication process and measurement analyzer. Then, the detailed experimental procedure of the MIM stacked structure is presented.

In Chapter 3, the factors to the resistive switching characteristics of the atomic-layer-deposited HfO_x thin film was investigated and discussed, including bulk HfO_x thin films, top electrode, the inserted reactive metal at the electrode/oxide interface, rapid thermal annealing in Ar and O_2 circumstance, process effect, and UV light irradiation. The electrode material, thickness, and fabrication process have to be well chosen for a more reliable switching behavior. For the HfO_x film, when the stacked metal Pd/Al was used as top electrode, both the unipolar and bipolar resistive switching characteristics can be performed for more than 1000 switching cycles under the continuously sweeping curves. Rapid thermal annealing under a controlled treatment time in oxygen ambient effectively improve the switching properties, while do no help on the switching characteristics in Ar circumstance. UV light direct irradiation on HfO_x surface can cause the oxygen-related defects or oxygen vacancies inside HfO_x film, which results in more random distribution on the conducting filaments. When ITO electrode was shielded above the HfO_x surface, an oxygen-riched HfO_2 layer could be formed at the M/O interface effectively modulate the switching properties and reduce the dispersion on switching parameters.

In Chapter 4, we discuss on the electrical characteristics of the Gd_2O_3 thin film, which were fabricated under different substrate temperature during the pulsed laser deposition (PLD). The Si-based and glass-based Gd_2O_3 devices were both investigated here. The resistance switching behaviors of $Ti/Gd_2O_3/Pt$ devices are highly correlated with the anode electrode. The switching characteristics operating under positive bias exhibits stable switching characteristics of 100 switching cycles with low voltage and resistance dispersion, while the switching characteristics becomes unstable and turn into a large fluctuation on resistance and voltage values when the devices are operated under negative bias. The other is the highly transparent RRAM devices based on $ITO/Gd_2O_3/ITO$ sandwiched structure. The Gd_2O_3-based T-RRAM device exhibits excellent bipolar resistance switching, good endurance of more than 1000 cycles, and multi-level states properties. A possible switching mechanism based on the migration of the oxygen ions between the interfacial layer and Gd_2O_3 film dominating the state to LRS or HRS under applied bias. Based on the results of XPS analysis, the different composition ratio on the metallic (Gd^0) / oxidized (Gd^{3+}) was calculated to be 65.5 % / 34.5 % and 49.3 % / 50.7 % for the 25 °C and 300 °C-deposited samples, respectively. The large amounts of defect in the Gd_2O_3 film, including oxygen vacancies or metal atoms, etc., may greatly dominate the switching characteristics.

In Chapter 5, we will first discuss the fabrication process effect on the thin film morphology, surface roughness, crystallinity, and material composition by varying oxygen pressure during PLD process of the amorphous LAO film. Then, the electrical characteristics of the three samples, such as leakage current, breakdown voltage, temperature effect to conducting current, and conducting behavior were also discussed. We observed that all the samples in LAO films during the electroforming process follow the three conduction mechanism: Hopping conduction → Schottky emission → Frenkel-Poole emission, as the applied voltage increases to breakdown voltage (V_{BD}). To explain why samples grown under different oxygen pressure during LAO films deposition will cause different electrical characteristics, voltage/resistance dispersion and its physical mechanism, the forming process is the key factor to be discussed. The residual electrons inside LAO contribute to the space-charge-limit conduction during the RS operation. LAO films grown at higher oxygen partial pressure is beneficial for a more reliable resistive switching performance, because the formation of the interfacial layer and lower oxygen vacancy concentration exist in the LAO thin film. The interfacial layer can serve as a good oxygen reservoir residence and the more oxygen ions involve can ensure the switching reliability. A blocking layer growth between LAO and ITO (BE) terminate the extended defects, which leads to a uniform distribution on the oxygen vacancy concentration from top to bottom insulator film.

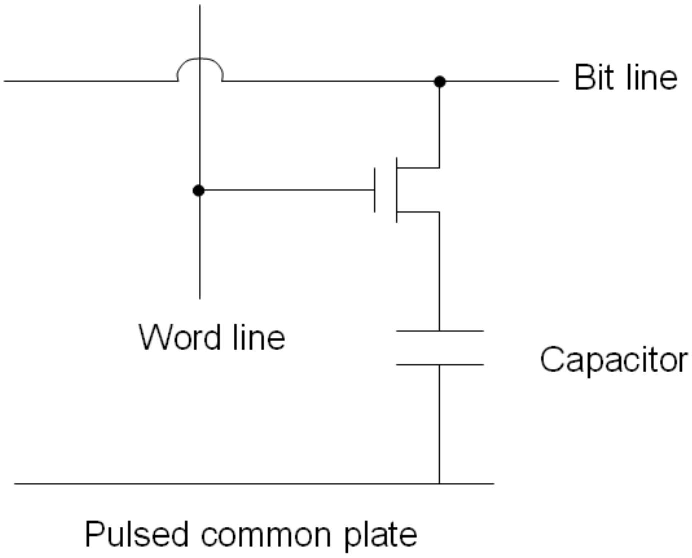

Fig. 1-1 DRAM cell with 1T1C structure.

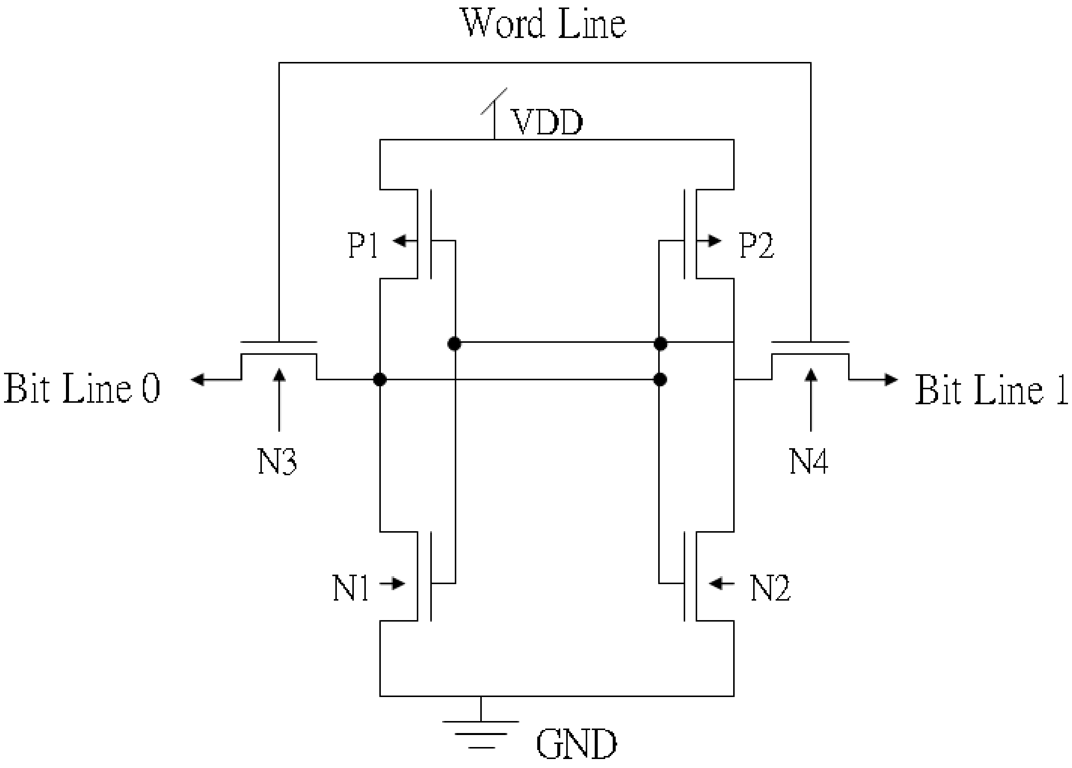

Fig. 1-2 SRAM CMOS cell with six-transistor (6T) configuration example

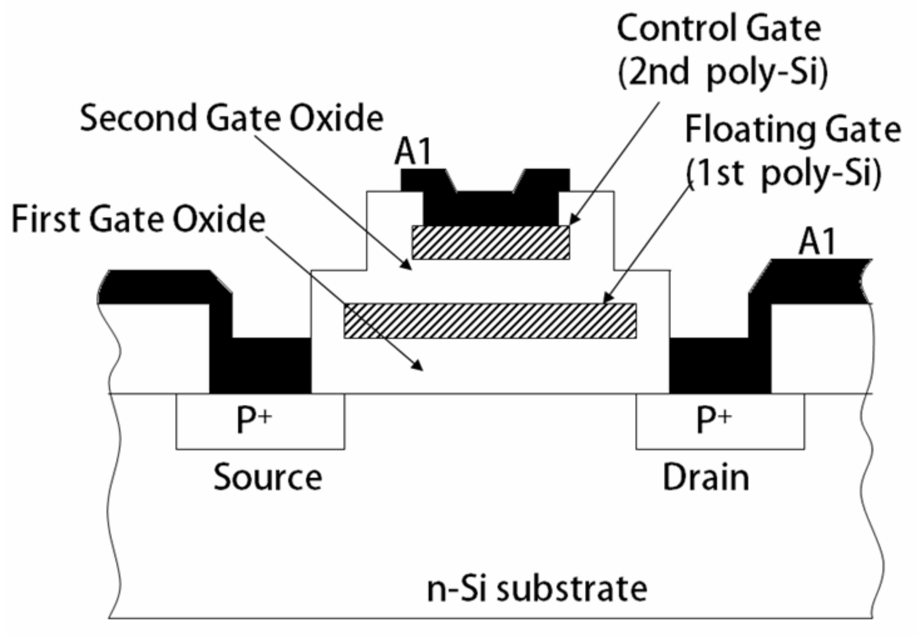

Fig. 1-3 Schematic cross section of a floating-gate Flash memory

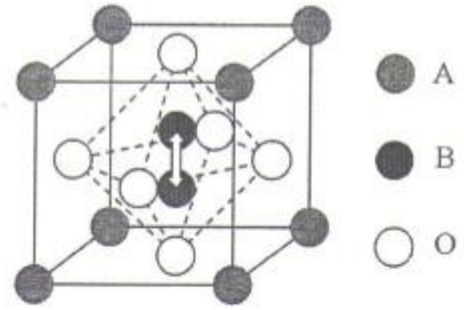

Fig. 1-4(a) The ferroelectric compositional structure of a perovskite crystal unit cell.

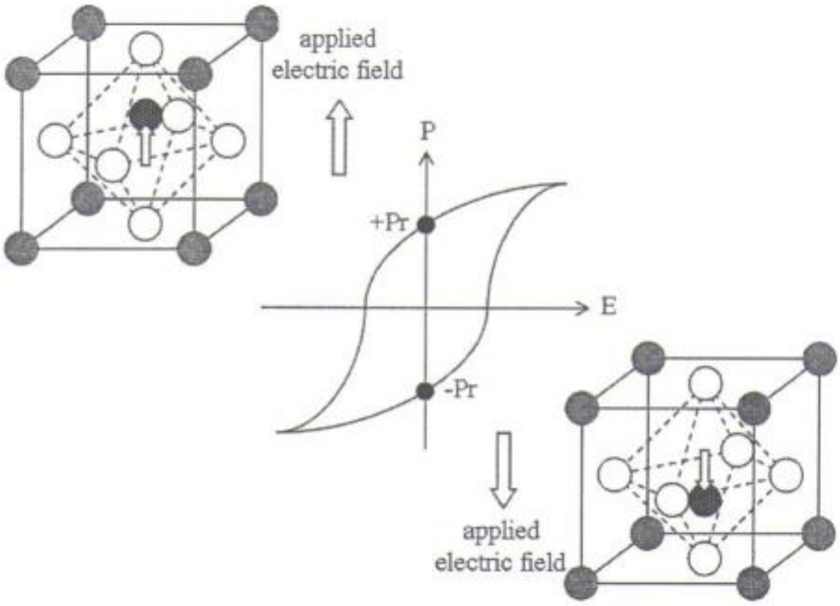

Fig. 1-4(b) The schematic diagram of the typical hysteresis curve related to the moving atoms under the applied bias.

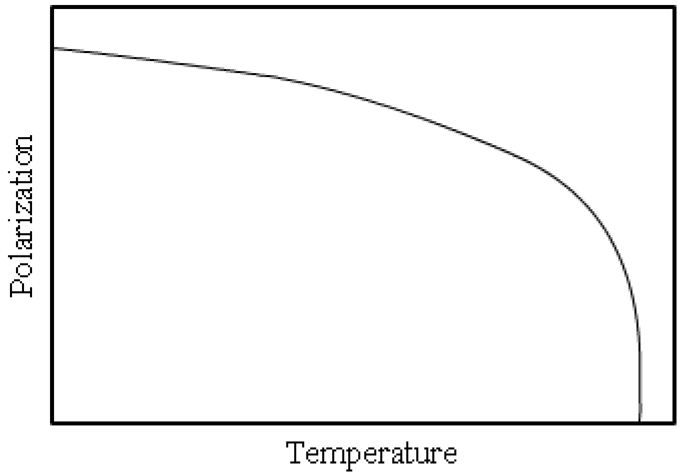

Fig. 1-4(c) Polarization versus temperature curve.

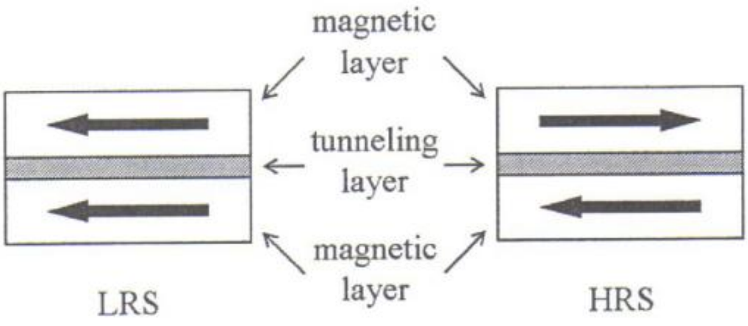

Fig. 1-5 Illustration of the low resistance state (parallel direction) and high resistance state (antiparallel direction) of the MRAM device.

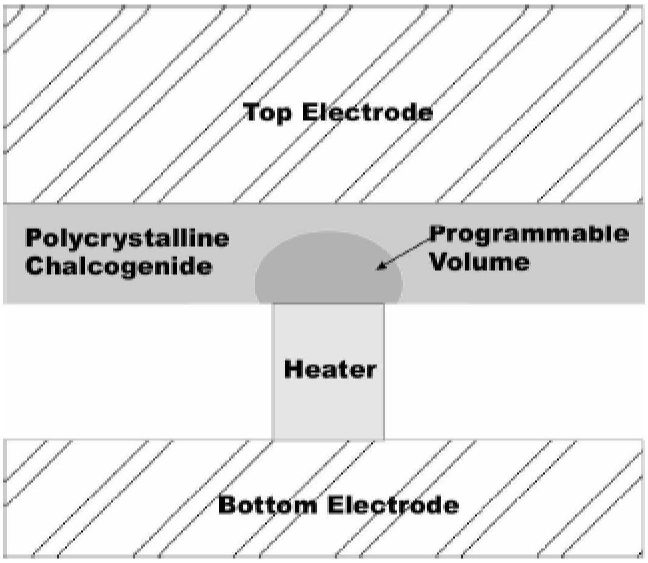

Fig. 1-6(a) Schematic diagram for the phase change memory cell consisting of $Ge_2Sb_2Te_5$ material. [13]

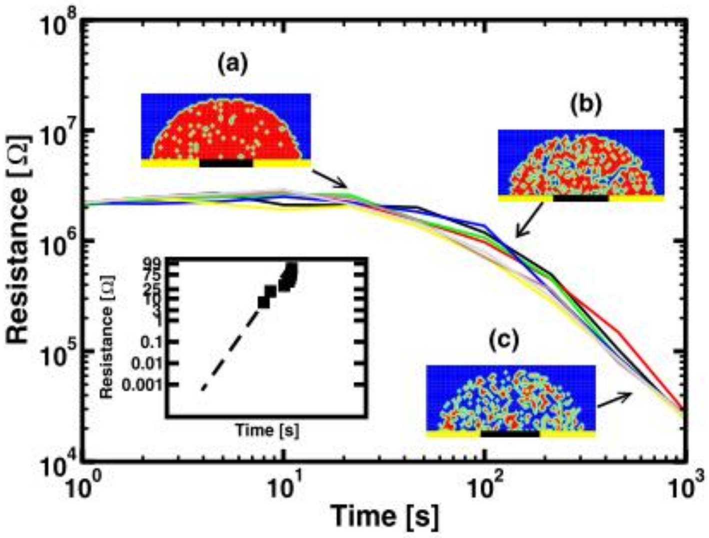

Fig. 1-6(b) According to the Monte Carlo model simulation for crystallization, the phase change in resistance values as a function of time can be shown. Crystal grains are in blue, amorphous phase in red. [14]

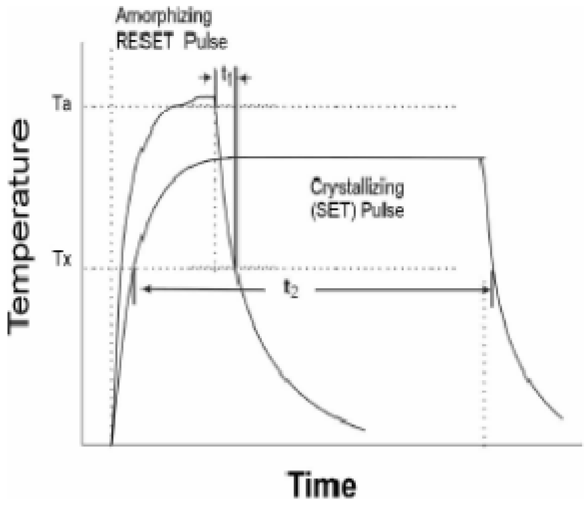

Fig. 1-6(c) Temperature-time relationship in SET and RESET pulse operation. [13]

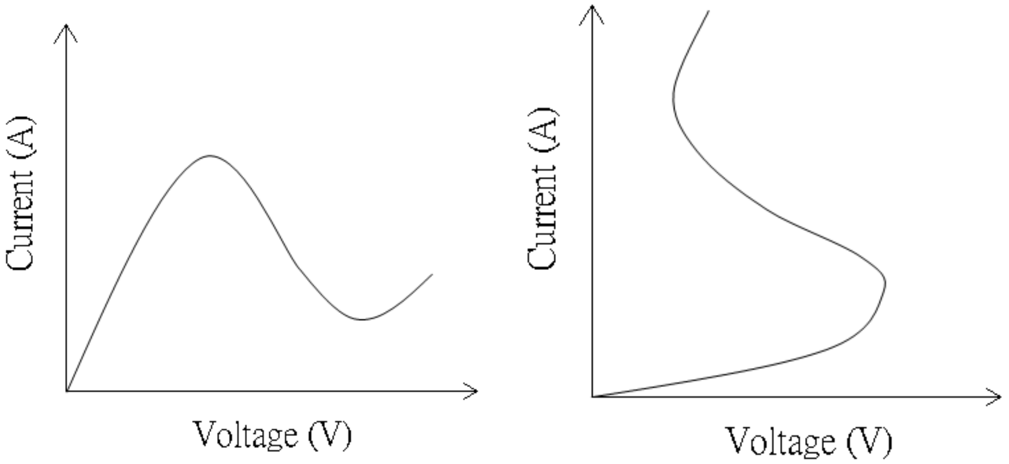

Fig. 1-7 Two types of differential negative resistance for (a) voltage controlled mode (N shape) and (b) current controlled mode (S shpae).

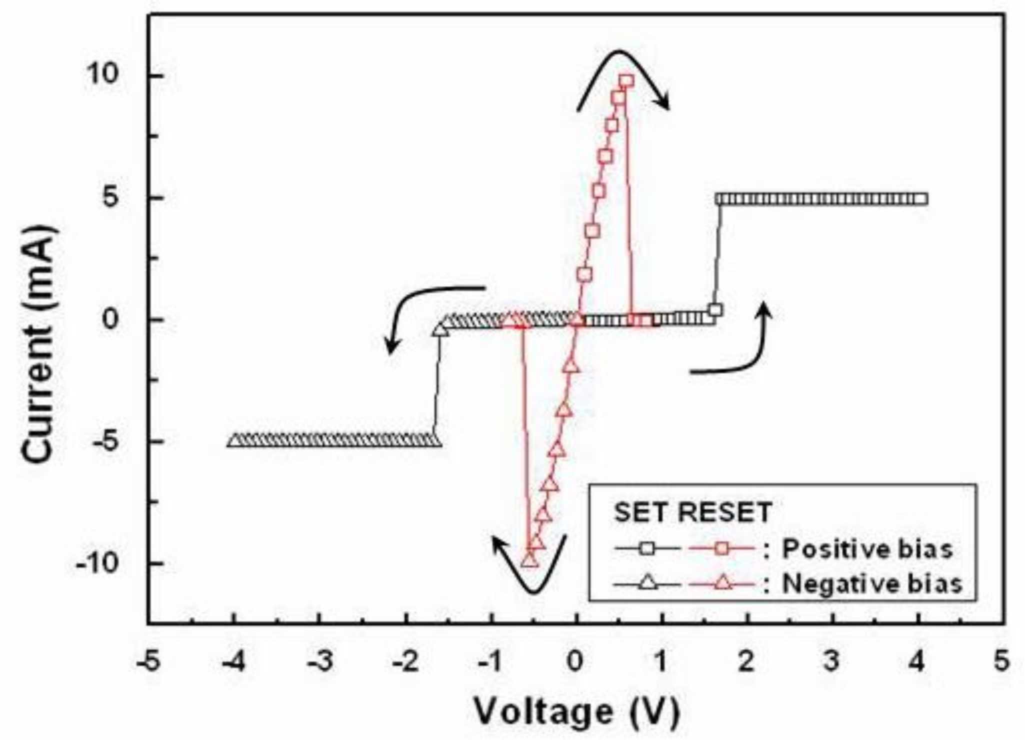

Fig. 1-8 The typical Unipolar I-V curves. The arrows indicate the sweep current loop.

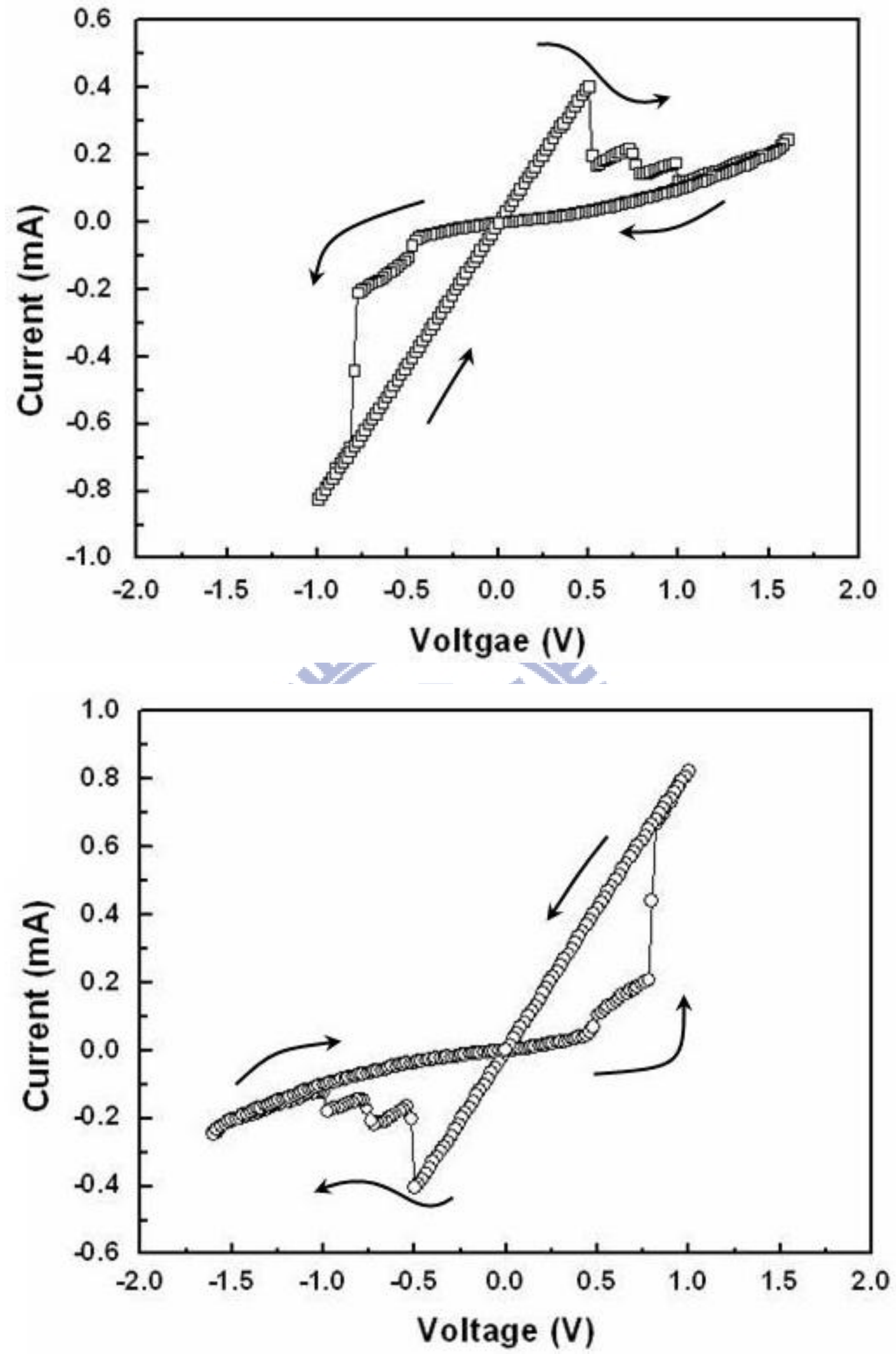

Fig. 1-9 The typical bipolar I-V curves at (a) clockwise current loop and (b) counterclockwise current loop.

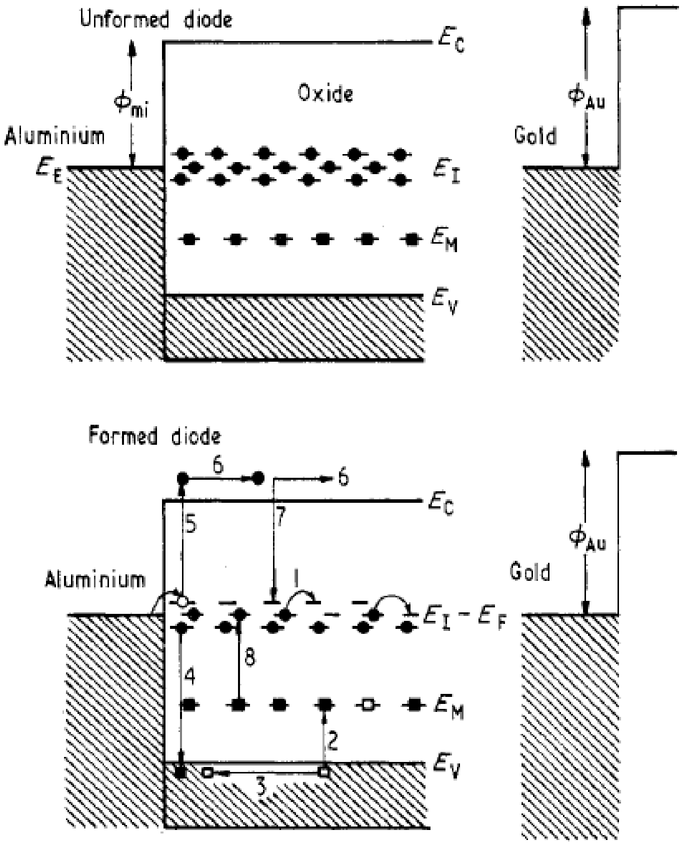

Fig. 1-10 Schematic illustration of conduction processes in the high-field region of a metal-oxide-metal structure. [15]

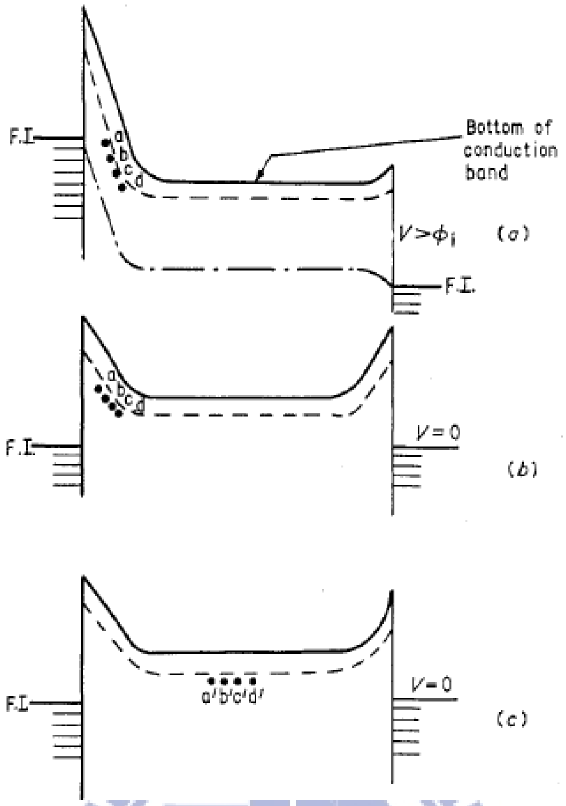

Fig. 1-11 Energy diagram showing the position of the stored charge relative to the Fermi level: (a) at a voltage bias of V volts, (b) immediately after voltage has been rapidly reduced to zero, (c) after a longer time interval. [16]

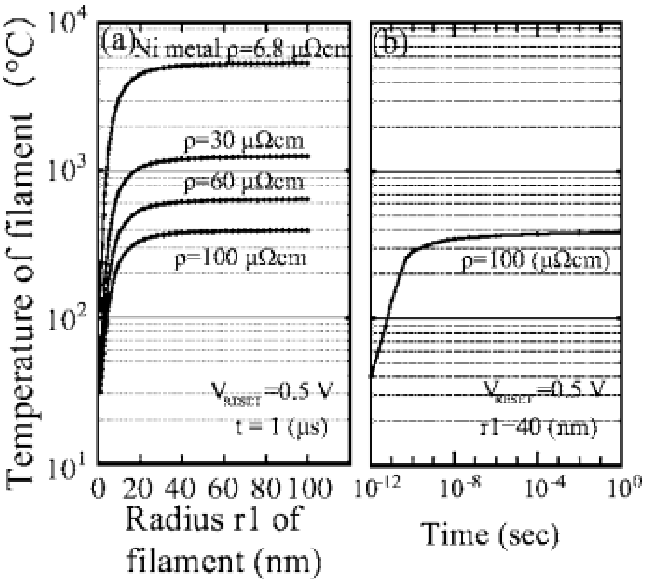

Fig. 1-12 (a) Temperature of filament as a function of filament radius with different resistivity values. (b) The relation between temperature of filament and measured time for 40 nm radius and resistivity = 100 μΩ. [19]

Material	Model	Equation	Condition	Heating temperature	Ref.
NiO	Steady state temperature model	$T_m = \left(T_o^4 + \frac{J^2 \rho r}{2P_w}\right)^{1/4}$	I=200 nA, r=5 nm, $\rho=5\text{x}10^{-4}\ \Omega\text{cm}$	720 K	[18]
NiO	thermal chemical reaction model	$\Delta T = \frac{1}{(K_R + K)} \frac{V_{reset}^2}{R}$	ρ=30 ρΩ, r=20 nm	1000 °C	[19]
Cu_2O	field-induced barrier lowering	$\Delta E\, \alpha \sqrt{qF/\pi\varepsilon}\,(eV)$	V~0.7V, t=12 nm, F~0.6 MV/cm, ΔE~0.2 eV	800 °C	[20]

Table. 1 Comparison on the estimated heating temperature of different material.

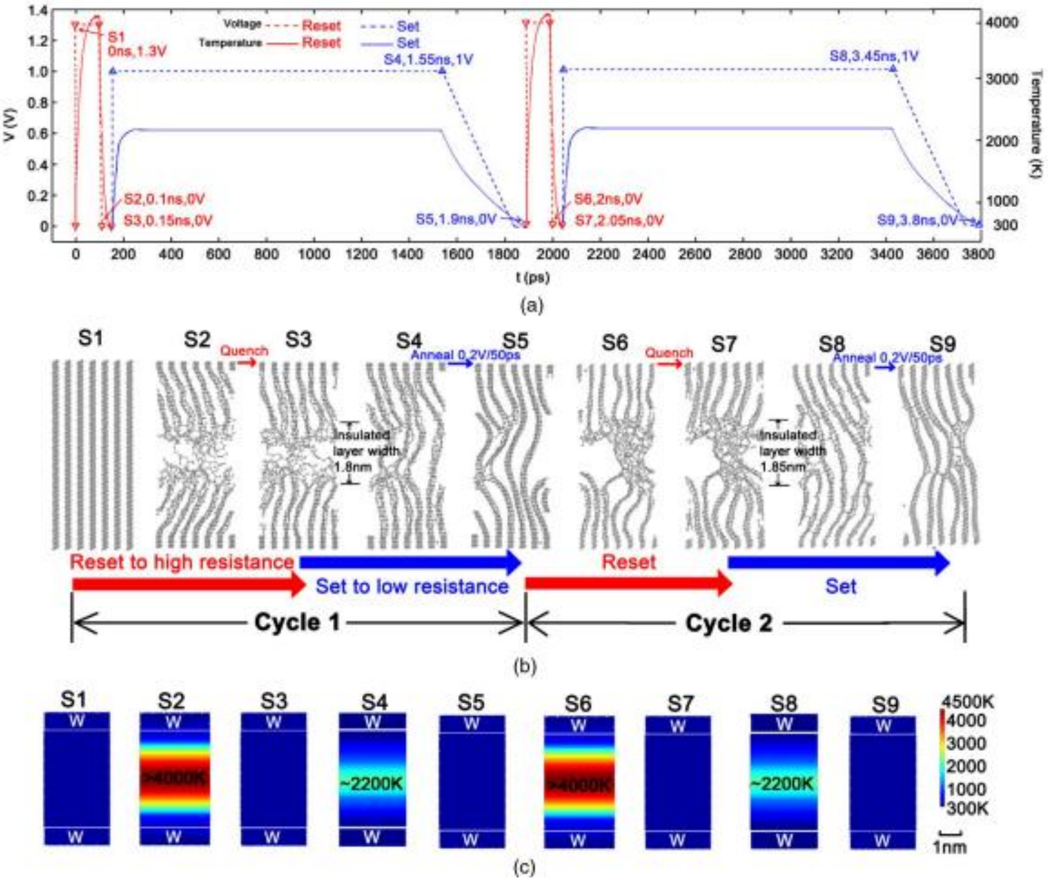

Fig. 1-13 Simulation test on two reset/set cycles of C-RRAM. (a) the applied voltage as a function of temperature, (b) distribution of the atomic structure in the simulated filaments, and (c) temperature distribution among the entire TMO film. [21]

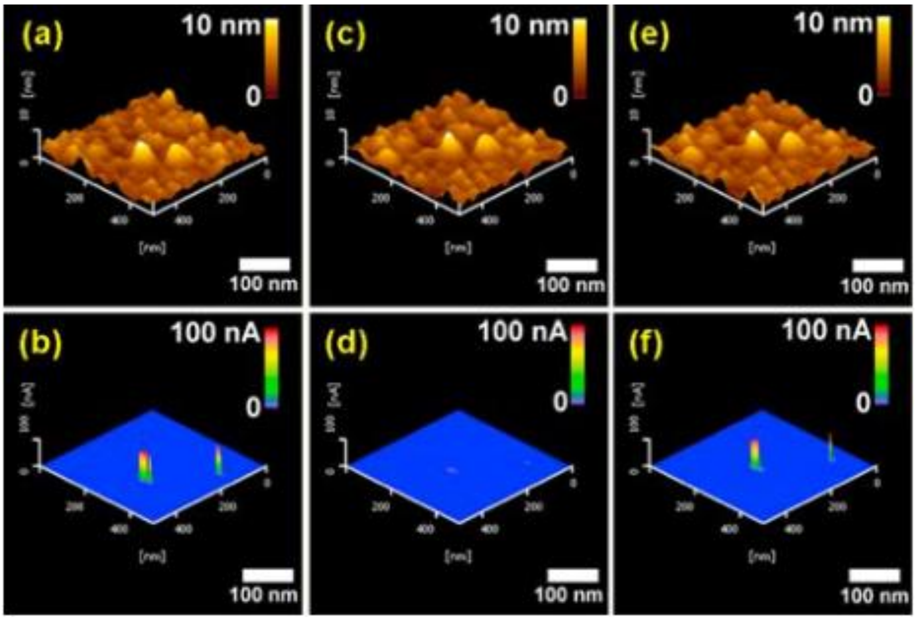

Fig. 1-14 Surface morphology (a),(c),(e) and its corresponding current images (b),(d),(f) are shown by AFM and C-AFM measurement, respectively. Operation condition of the (a)(b) SET scan under 2.3 V bias, (c)(d) RESET scan under 1.5 V bias, and (e)(f) SET scan under 2.3 V bias. [32]

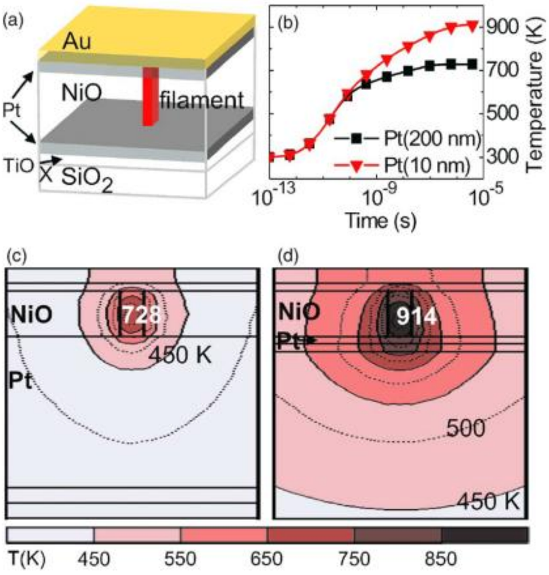

Fig. 1-15 (a) A schematic diagram showing the sample geometry. (b) Simulation on temperature as a function of measured time at the filament center under applied bias. Temperature distribution for the case with (c) 200 nm and (d) 10 nm bottom Pt electrode. [33]

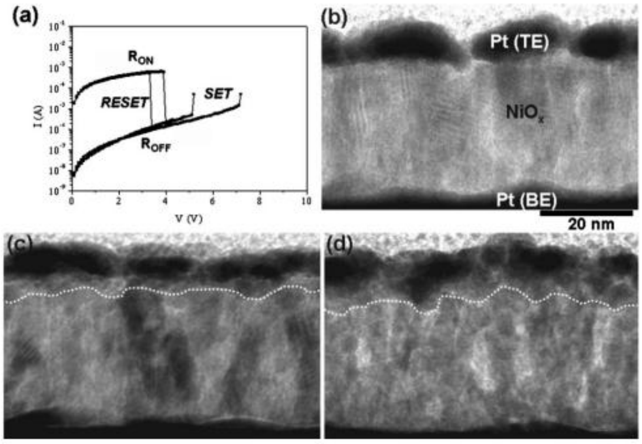

Fig. 1-16 (a) Typical I-V curve of NiO film. Cross-sectional TEM images of the Pt/NiO/Pt structure of (b) pristine, (c) LRS, and (d) HRS. [18]

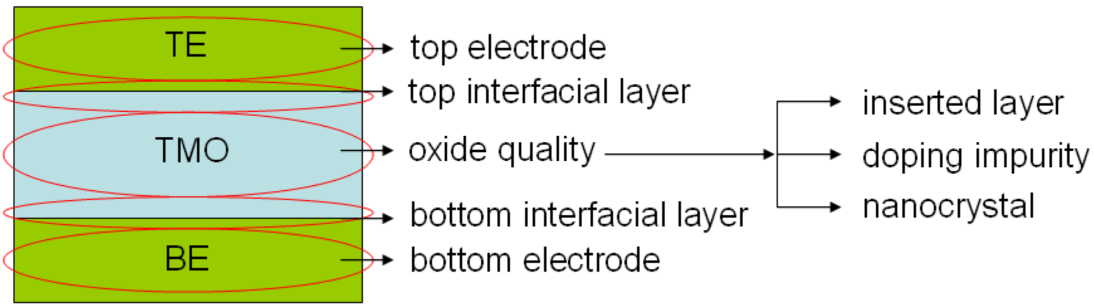

Fig. 1-17 Schematic diagram of the MIM stacked structure.

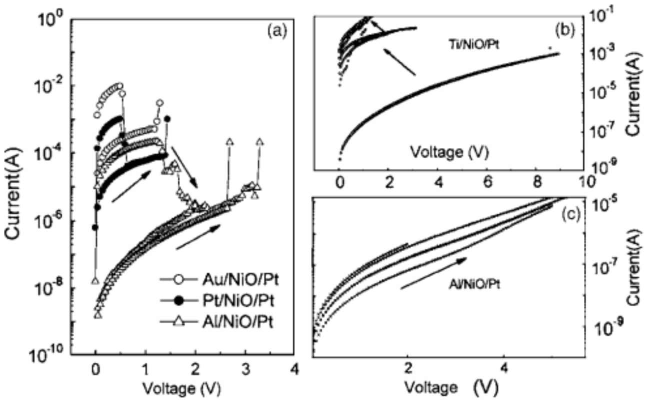

Fig. 1-18 (a) Resistive switching test of NiO films with Au, Pt, or Al as top electrode. (b) Al/NiO/Pt and (c) Al/NiO/Pt structures. The arrows indicates the sweeping directions of applied bias. [35]

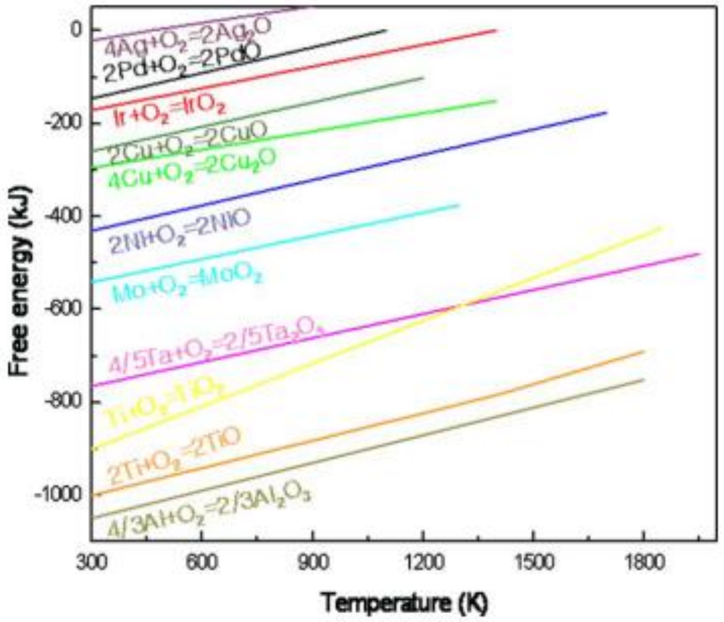

Fig. 1-19 Ellingham diagram reveals the free energies for oxidation of the various metals. [37]

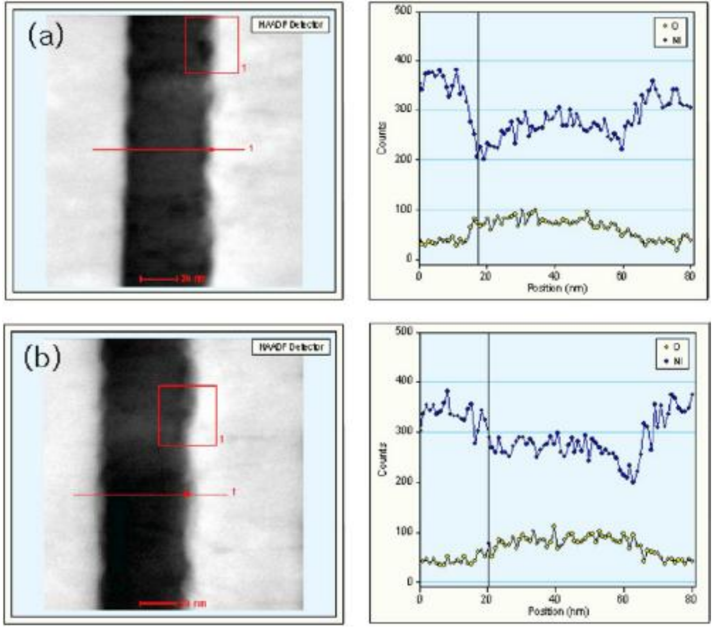

Fig. 1-20 Cross-sectional TEM image and corresponding EDX analysis of NiPt/NiO/NiPt thin film (a) beform forming and (b) after forming. Ni penetration into the NiO film after forming process was clearly observed. [57]

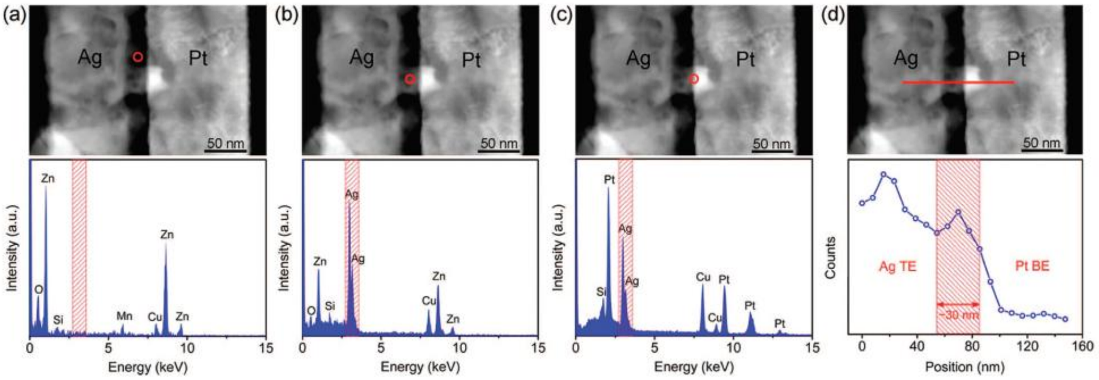

Fig. 1-21 The EDX analysis in STEM mode for detection on the atomic materials. Four places were detected for investigation the Ag bridge involving inside the TMO films. (a) out side the Ag bridge, (b) in the middle of the Ag bridge, (c) near the Pt electrode, and (d) a line profile for showing the intensity of Ag atoms along the bridge. [94]

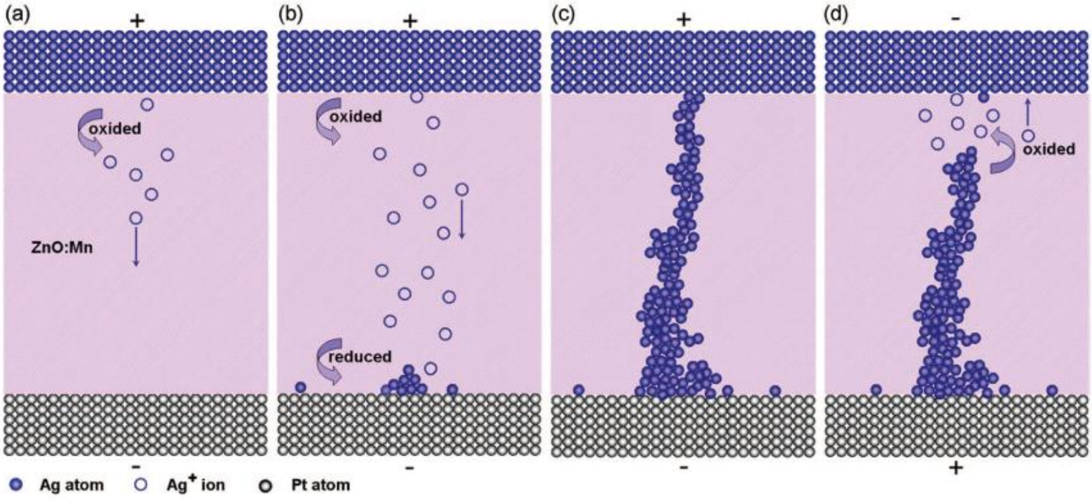

Fig. 1-22 A schematic diagram for the resistive switching mechanism of the electrometallization memory. (a) Oxidation of Ag atoms at anode, (b) migration of Ag cations toward the cathode and their reduction process, (c) The precipitations of Ag atoms connect the anode and cathode and form a metallic Ag conducting bridge. And (d) the electrochemical dissolution of Ag bridge takes place. [94]

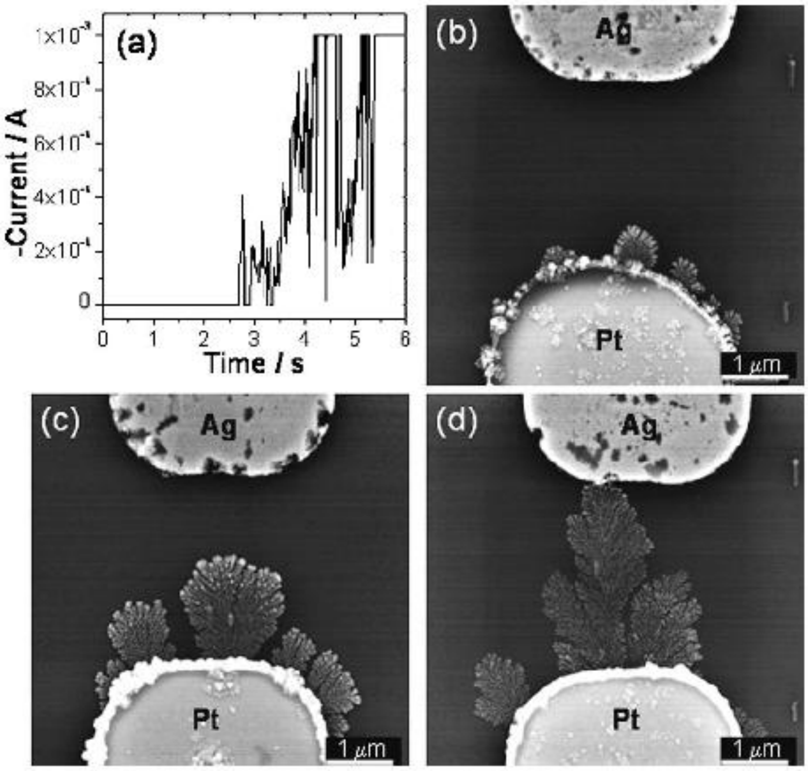

Fig. 1-23 SEM images showing the Ag dendrite growth under the applied bias of -1 V for about (a) 0 s, (b) 1 s, (c) 2 s, and (d) 4 s, respectively. [98]

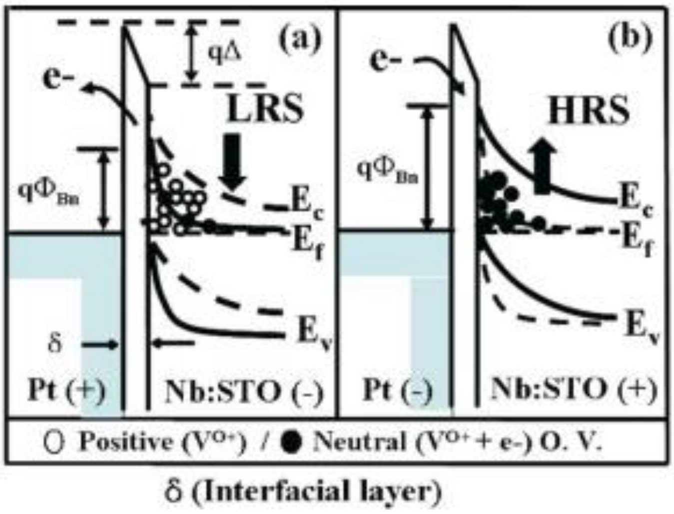

Fig. 1-24 Schematic diagram of Pt/Nb:STO Schottky junction for indicating the Schottky barrier height modulated by the trapped electrons. [105]

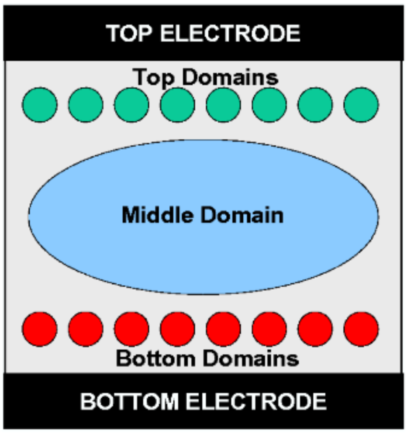

Fig. 1-25 Schematic diagram of the three domains model. The insulator film can be regarded as top, middle, and bottom domains, respectively. The tunneling amplitudes between two domains regulate the injected carriers. [119]

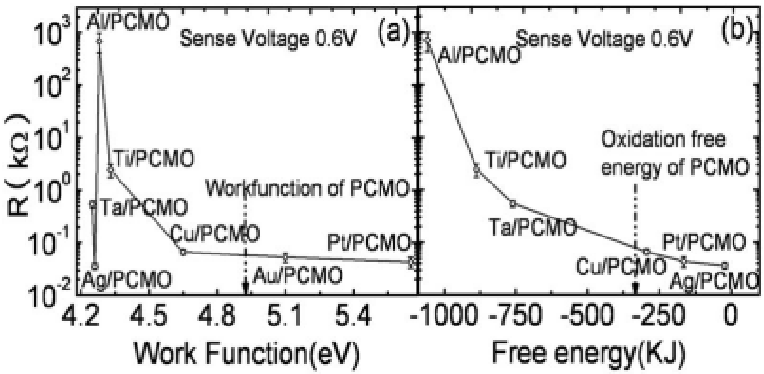

Fig. 1-26 (a) virgin resistance vs. WF, and (b) virgin resistance vs. free energy. [142]

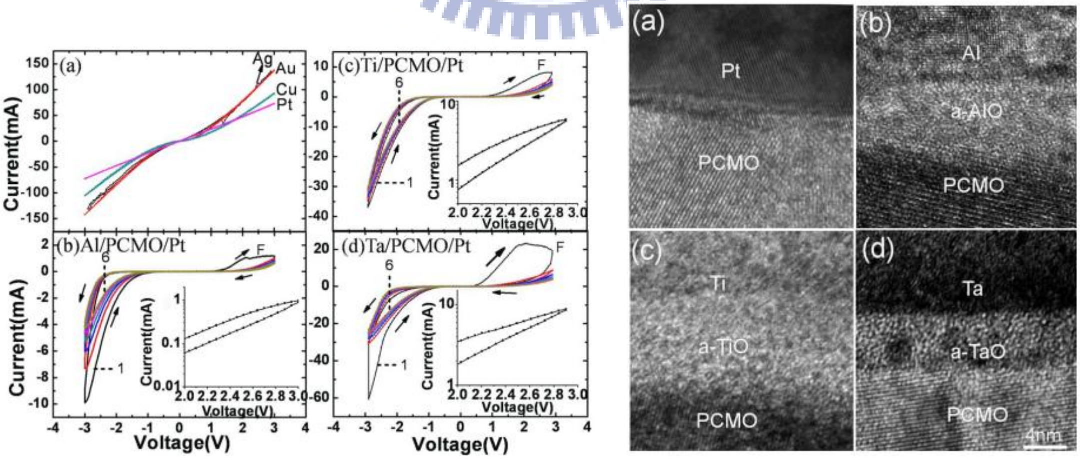

Fig. 1-27 I-V characteristics for (a) Ag, Cu, Au, Pt/PCMO/Pt, (b) Al/PCMO/Pt, (c) Ti/PCMO/Pt, and (d) Ta/PCMO/Pt. The switching loop is followed by 0 V → 3 V → -3 V → 0 V. The cross-sectional HRTEM images at right side are the corresponding microstructure. [142]

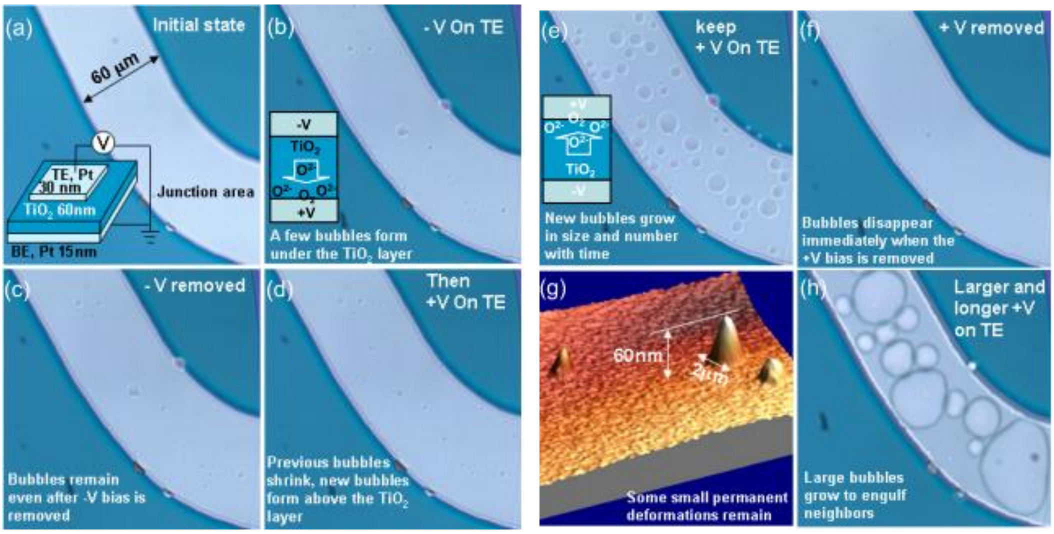

Fig. 1-28 Bubble gas observation at (b),(c) negative bias, then at (d)-(h) positive bias. (g) The eruption features observed by atomic force micrograph after bias voltage was removed. [191]

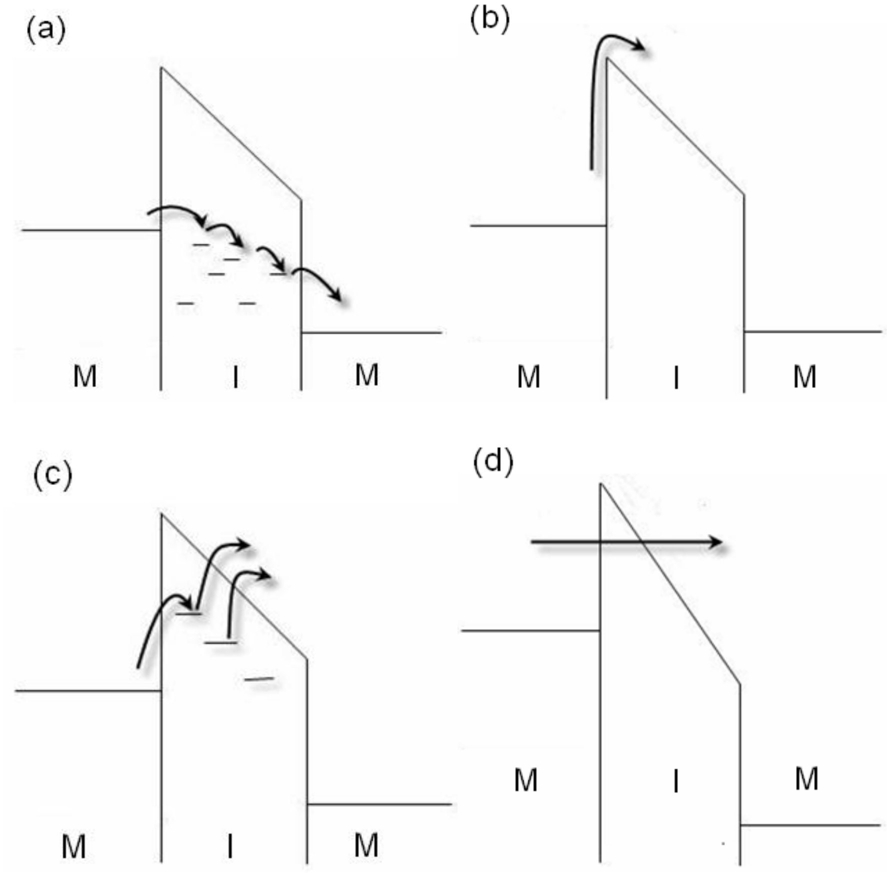

Fig. 1-29 The schematic diagram is shown for (a) ohmic conduction, (b) Schottky emission, (c) Frenkel emission, and (d) Fowler-Nordheim Tunneling.

Chapter 2 Experimental details

2.1 Introduction of Pulsed Laser Deposition

The application of pulsed-laser deposition (PLD), a technique to deposit thin films of complex materials, is growing exponentially. The success of PLD in the deposition of a wide variety of materials has spurred research interest in this technique world wide. In 1965, Smith and Turner conducted the first experiment on PLD; the authors used a ruby laser to deposit thin films on semiconductors, dielectrics, chalocogenides, and organometallic materials. In 1987, Dijkkamp et al. succeeded in growing *in situ* high-temperature superconducting films by PLD, which brought an overwhelming interest to this field. Although Zeitsev-Zotov et al. first demonstrated the perovskite-type superconductor in 1983, the process was further improved by the Bellcore group, which provided the catalyst that initiated an explosive growth in PLD research interest. PLD is a simple and versatile experimental setup, which makes it an affordable technique for exploring new frontiers in material science. In the following, we will introduce the equipment setup of PLD and the mechanism of process deposition.

2.1.1 PLD equipment setup

The basic equipment required to begin work in PLD, including the following: lasers, optics, and deposition systems.

(a) Lasers

Gnerally, the useful range of the laser wavelengths for thin-film deposition by PLD is approximately 200 and 400 nm. The laser wavelength comes into play mainly in effectively absorbing laser power into the target. Absorption coefficients tend to increase as one moves to the short wavelength end of this range and the penetration depths into the target materials are correspondingly reduced. This is a favorable situation because a thinner layer of the target surface is ablated as one moves closer to the 200 nm mark. Below 200 nm, strong absorption by the Schumann-Runge bands of molecular oxygen can make working in this part of the spectrum difficult. Bulk damage due to color center formation occurs easily at the shorter ultraviolet laser wavelengths.

Most of the PLD work accomplished to date has been centered around excimer laser (gas laser system) and the Nd3+:YAG laser (solid-state sytem) as the deposition source. KrF excimer laser is the popular choice among PLD system due to the highest gain system for electrically discharged pumped excimer laser. In the present experiment, KrF excimer laser was employed to perform the fabrication process. The excimer molecules were formed in a gaseous mixture of their component gases, such as Xe, HCl, and Ne in the case of the XeCl laser. Energy was pumped into the gas mixture through avalanche electric discharge excitation. The pumping created ionic and electronically excited species that reacted chemically and produce the excimer molecules.

(b) Optics

Optical elements are placed between the output port of the laser and the laser port of the deposition chamber to steer and focus the beam. The optical elements that couple the energy from the laser to the target are lenses and apertures; mirrors; beam splitters, and laser windows.

Lenses are the most important thing among the above-mentioned optical elements because the primary function of the lens is to collect radiation from the laser source and focus it to a precise point on the target surface to achieve the required energy density for ablation. In the PLD process, one of the most important deposition parameters that dominate the film stoichiometry and crystallographic quality is the laser energy density (J/cm^2) incident on the target. The lens material must be free of inclusions, bubbles and mechanical distortions. When using a KrF excimer laser at 248 nm, UV-grade fused-silica lenses are a good and cost-effective choice.

Mirrors are used in any PLD laboratory to share the expensive excimer laser to more than one deposition chamber efficiently. Furthermore, mirrors are used to reflect off the primary beam with the laser beam incident at an angle of 45° with respect to the normal to the mirror.

Beam splitter split the laser beam into two or more separate beams, an approach applied for a dual-beam chamber with mirrors. The dual-beam PLD is a method used to improve the characteristics of target erosion.

(c) Deposition chamber

Once the laser beam passes through the optical elements, it enters the deposition chamber. The foundation for a versatile PLD deposition system is composed of the following elements: chamber, target manipulation, substrate holder and/or heater, gas flow, and vacuum gauging.

The schematic PLD setup shown in Fig. 2-2 is an example of a setup that works well. Listed in the figure are the many critical and important parameters that needed to be considered when performing this deposition because they may dominate the quality of thin film. In Fig. 2-2, five dimensions are indicated: T is target port flange-to-beam focal plane (target) distance; Z is substrate port flange-to-substrate distance; S is target-to-substrate distance; L is laser port length; θ is angle between target normal (plume direction) and the laser beam.

The manipulation of the target is very flexible, and a PLD system only has a few intrinsic restrictions. Successful depositions can be made from pressed powders, sintered pellets, cast material, single crystals, and metal foils. The target surface roughness is critical to having a high-quality film, which can be freed from splashing.

As with most thin-film deposition techniques, the manner in which the substrate is held and its location and orientation relative to the target are important parameters in a PLD system. The target-to-substrate distance (*S*) depends on several factors, the most significant of which is the energy delivered to the target. Trade-off between the energy and *S* is a efficient way to obtain an optimal condition of the PLD process because the evaporant energy and deposition rate can be well controlled.

2.1.2 Mechanism of the PLD process

PLD process can be divided into the following four stages:

1. Laser radiation interaction with the target
2. Determination of the dynamic of the ablation materials
3. Deposition of the ablation materials with the substrate
4. Nucleation and growth of a thin film on the substrate surface

In the first stage, the laser beam is focused onto the surface of the target. At sufficiently high energy densities and short pulse duration, all elements in the target surface are rapidly heated up to their evaporation temperature. Materials are dissociated from the target and ablated out with stoichiometry as the target. The instantaneous ablation rate is highly dependent on the fluencies of the laser irradiating on the target. The ablation mechanisms involve many comples physical phenomena, such as collisional, thermal, and electronic excitation, exfoliation and hydrodynamics.

During the second stage, the emitted materials tend to move toward the substrate according to the laws of gas dynamic, and show the forward-peaking phenomenon. R.K. Singh reported that the spatial thickness varied as a function of cosnq, where

n>>1. The laser spot size and the plasma temperature have significant effects on the deposited film uniformity. The target-to-substrate distance is another parameter that governs the angular spread of the ablated materials. Hanabusa also found that a mask placed close to the substrate could reduce the spreading.

The third stage is important to determine the quality of thin film. The ejected high-energy species impinge on the substrate surface and may induce various type of damage to the substrate. These energetic species sputter some of the surface atoms, and a collision region is established between the incident flow and the sputtered atoms. Film grows immediately after this thermalized region is formed. The region serves as a source for condensation of particles. When the condensation rate is higher than the rate of particles supplied by the sputtering, thermal equilibrium condition can be reached quickly and film grows on the substrate surface at the expenses of the direct flow of the ablation particles.

The fourth stage is the nucleation-and-growth of crystalline films. It depends on many factors, such as the density, energy, ionization degree, and type of the condensing materials, as well as the temperature and the physical-chemical properties of the substrate. According to Greene, the conventional theory of film nucleation and growth states that the growth mechanism is greatly dominated by two main thermodynamic parameters: the substrate temperature T and the supersaturation m.

The nucleation process depends on the interfacial energies between the three phases present, namely, substrate, clusters and vapor. The minimum-energy shape of a nucleus resembles a cap. The critical size of the nucleus depends on the driving force, that is, the deposition rate and the substrate temperature. For a large nuclei - a characteristic of small supersaturation - isolate patches (islands) of the film on the substrates are created, which subsequently grow and coalesce together. As the supersaturation increases, the critical nucleus shrinks until its height reaches an atomic diameter and its shape is that of a two-dimensional layer. For large supersaturation, the layer-by-layer nucleation will happen for incompletely wetted foreign substrates.

2.2 Introduction of Atomic Laser Deposition

Atomic layer deposition (ALD) is a new technique for producing thin films that is making headway into semiconductor manufacturing industry. ALD provides an easy way to produce uniform, crystalline, high quality thin films, especially to layered structures such as superlattices and superalloys. It is a chemical vapor deposition (CVD) method of depositing thin films, where precursor molecules are pulsed into a chamber and react to cover the substrate. Due to saturated surface reactions, ALD can be easily controlled to an accuracy of a single atomic layer. A purge gas is introduced to the chamber to remove unreacted precursors. A pulse of oxidant deposits oxygen and removes the precursor ligands, and another purge step is repeated. This series is repeated to build up a film. ALD is known for its ability to produce uniform, conformal films with precise control of thickness. The self-limiting growth mechanism of ALD is that the final thickness of the thin film, which depends only on the number of deposition cycles.

2.3 Evaporation system

In this process, the source material is heated in a vacuum chamber which has initially been pumped down to 10^{-5} torr. Evaporated atoms from the source condense on the surfaces of the wafers. The heater can be fabricated by using a tungsten filament as the resistance type, which heats up when current passes through it. Most of the microelectronics is use an e-beam heater, which a high-energy electron beam is focused onto the source material in a crucible controlled by magnetic fields. This process by using e-beam heater can provide clearner thin film quality and no metal contaminants such as sodium and potassium was found during Al evaporation systems. This evaporation deposition process based on the following steps: e-beam heater evaporates the Al ingots, then the Al gas transported through a high-vacuum chamber and deposited on wafer holder. Because the source is a point spot, one can determine the location of source and wafers to achieve the uniform deposition with an ideal point source, ideal cosine emission with a small planar surface source, or non-ideal and anisotropic emission with a small planar surface source. The evaporation process is an easy, cheap, and low cost technique. There is little damage caused to the wafer because the wafers do not suffer the energetic particles bombardment. Deposited thin films are pure due to the process is done under a high vacuum. However, several problems hinder the application in semiconductor fabrication, including difficulty in depositing alloys, compounds, and high-vapor pressure elements, lack of an in situ preclean, and poor step coverage.

2.4 Sputter system

In the sputter system, an inert gas such as Ar, is fed into the sputtering chamber. A voltage bias applied across the two electrodes is needed to create the plasma. The plasma contains neutral argon atoms, and roughly equal numbers of positive ions and free electrons, and is conducting medium. The negativd voltage is applied to the top electrode and the sputtered target was placed on this side, therefore, the electrode was named as cathode electrode or the target. The wafers put on the opposite side - bottom electrode, which was a metal platen and maintained grounded. The voltage bias can create the plasma charges, and then the negative bias voltage attracts the energetic ions to strike the target and sputter the target atoms. These sputtered particles will transfer across the plasma as a vapor and strike the wafer surface, then condense and form the deposited film. The target or source material acts as an electrode during sputter deposition, therefore, a conductive material such as metals can be sputtered in DC mode sputtering deposition. For the nonconductors, such as oxide or nitrides, the RF or AC mode of sputter deposition system is needed.

2.5 Fabrication of resistive switching memory devices

2.5.1 Deposition of HfO_x RRAM devices

(a) Substrate and bottom electrode

Resistive memory devices based on HfO_x capacitor structure were fabricated as follows. The p-type 4-inch Si (100) wafer was cleaned by the standard RCA cleaning process. Then, a 300-nm-thick SiO_2 layer, served as an isolated layer to prevent the leakage current from Si substrate, was grown on the Si wafer by wet oxidation at 1000 °C. TiN metal as a bottom electrode was deposited onto the SiO_2 layer by sputtering.

(b) HfO_x thin film

Resistive memory devices were fabricated as follows. TiN metal as a bottom electrode was deposited on an 8 inch Si wafer by sputtering. Then, nonstoichiometric HfO_x films were deposited by atomic layer deposition (ALD) (ASM, Polygon 8200) at temperature of 300 °C. Hafnium tetrachloride ($HfCl_4$) and water (H_2O) with a compositional ratio of 5:2 and 5:3 were both used as reactants for HfO_x deposition. The primitive chemical-formula is shown as follows.

$$HfCl_4 + 4H_2O \rightarrow Hf(OH)_4 + HCl \uparrow \qquad (2\text{-}1)$$

$$Hf(OH)_4 \text{ heating} \rightarrow HfO_2 + H_2O \qquad (2\text{-}2)$$

(c) Top electrode

For a universal understanding of the switching properties of HfO_x thin film, we not only fabricated various kinds of electrode materials but also varied different deposition condition during top electrode deposition.

First, we discuss the top electrode effect on the resistive switching properties as discussed in section 3.3.2. Various kinds of metals as top electrodes were deposited by dc sputtering using a shadow mask at room temperature, such as Pt, Pd, Cu, Ni, Ti, Al and etc. The thickness of metals was varied from 30 to 100 nm. The circular top electrodes were formed with radiuses of 100-800 μm.

In section 3.3.3, for a further investigation on the effect of the reactive metal Al, the stacked top electrodes Pt/Al were also fabricated with the thickness of Al varied from 0.5-10 nm and capping a 30 nm thick Pd electrode above. To maintain high quality of metal Pd/Al interface, we deposited the stacked film in the same chamber. The pure Pd metal with 30 nm thick was also deposited for comparison. The RF sputtering power and deposition pressure were kept at 30 W and 3 mtorr, respectively. Only argon gas (Ar, 99%) was used as the sputtering gas during deposition. Shadow mask with a diameter of 200 μm was used as the defined contact pad for measurement.

In section 3.3.5, we compared the process effect on the switching characteristics. Dc magnetron sputtering and/or e-beam evaporation were both used for Pt deposition as top electrode through shadow mask with a diameter of 200 μm. The operating current, voltage and working pressure for e-beam evaporation were 0.4 mA, 3 V, and 9×10^{-6} torr, respectively. Where sputtering was used on the Pt target (99.99%), minutes under the same gas composition as for the deposition to establish a steady state. The base pressure for sputtering the Pt top electrode was 2×10^{-6} torr using a cryopump and the working pressure of Ar gas (99.99%) was kept at 7×10^{-3} torr in all samples during the deposition process. The distance between the target and substrate was kept at 13 cm. For the stacked electrode, the thin Pt layer, with a thickness of 5 nm or 15 nm, was deposited by e-beam evaporation first, followed by a 70 nm thick Pt electrode with sputtering power of 100 W, while keeping all the process parameters the same. Sputtering power was varied between 50 W (94 V, 0.53 A), 100 W (161 V, 0.62A), and 200 W (237 V, 0.84 A) to investigate the effect of different levels of sputtering power on the electrical characteristics. Pt metal was deposited by e-beam evaporation (Pt (E)) or dc sputtering (Pt (S)) and electrically analyzed. Furthermore, stacked pt electrode samples, consisting of a thin Pt layer with a thickness of 5 nm or 15 nm deposited by e-beam evaporation followed by a 70 nm-thick Pt layer deposited by dc sputtering, were denoted as Pt (E50+S) and Pt (E150+S), respectively.

In section 3.3.6, we used the transparent electrode ITO as top electrode to investigate the impact of the UV laser on the switching properties. ITO with a thickness of 100 nm was deposited by rf-magnetron sputtering using a shadow mask with a 200 μm diameter at RT. The ITO film directly deposited on the glass substrate was also experimented on to measure the transmittance. The flow rate of the Ar sputtering gas was maintained at 15 sccm during deposition. Deposition power of 100 W and process pressure of 5 mtorr were used. An average intensity of 80 mW/cm^2 at = 365 nm of UV light from a mercury lamp was used in our experiments. The UV-light source was 8 cm away from the samples. UV-light exposes on the HfOx/TiN sample was experimented inside glove box, which requires oxygen and moisture concentration below 1 ppm. Exposure time of 30, 120, 300 and 600 seconds was adopted to perform the experiments.

(d) Treatment

After HfOx film deposition, some samples were thermally annealed in a rapid thermal annealing (RTA) system at 400 or 500 °C for 30, 60, 90, and 120 seconds.

Argon (Ar) and oxygen were used as annealing gas for the annealing systems. Then, nickel (Ni) as a top electrode was deposited by e-beam evaporation using a shadow mask at RT. The thickness of Ni and diameter of top electrode was 50 nm and 500 μm, respectively. The topic is discussed in section 3.3.4.

2.5.2 Deposition of Gd_2O_3 RRAM devices

(a) Experimental details of Ti/Gd_2O_3/Pt RRAM devices

For the Si based Gd_2O_3 RRAM, the p-type 4-inch Si (100) wafer was cleaned by the standard RCA cleaning process. Then, a 300-nm-thick SiO_2 layer, served as an isolated layer to prevent the leakage current from Si substrate, was grown on the Si wafer by wet oxidation at 1000 °C. A bilayer metal Pt/Ti was deposited on SiO_2 layer as a bottom electrode by e-beam evaporation. Thin metal Ti was used to enhance the adhesion of Pt electrode on SiO_2 layer. A 25 nm-thick Gd_2O_3 thin film was then deposited on Pt/Ti/SiO_2/Si substrates at room temperature (RT) by pulsed laser deposition (PLD) with oxygen pressure of 0.01 Pa using a metal Gd target. Finally, the bilayer electrode Pt/Ti was deposited on Gd_2O_3 as the top electrode. Shadow mask with a diameter of 200 μm was used to define contact pad for measurement.

(b) Experimental details of the ITO/Gd_2O_3/ITO T-RRAM devices

For the transparent RRAM, we use commercial ITO glass with as our bottom electrode and substrate. Then, we use PLD to deposit Gd_2O_3 using ceramic Gd_2O_3 target as the resistive layer of TRRAM device at room temperature (RT), 200 °C, and 300 °C. Lambda physics of excimer layser was furnished by λ=248 nm, pulse duration of 25 ns, repetition rate of 3 Hz, and the laser energy of 500 mJ. The process parameter of oxygen pressure is 10 mtorr and the thickness is controlled to 25 nm. At last, we also use ITO as a top electrode, a 100 nm-thick ITO thin film is deposited by dc sputter system using a shadow mask with a diameter of 1200 μm.

2.5.3 Deposition of LAO T-RRAM devices

The commercial ITO (Corning 1737) glass substrates deposited with 300-nm-thick transparent conducting indium tin oxide (ITO) thin films prepared as the bottom electrode. Then, PLD was used to deposit the LaAlO using LaAlO target as the resistive layer of T-RRAM device. A KrF excimer laser (λ=248 nm) was used as the light source of PLD with a pulse duration of 25 ns, a repetition rate of 3Hz, and a laser energy of 500 mJ. The distance from the target to the substrate was 10 cm and the target rotation rate was 5 rpm. The ambient oxygen pressure, which is the most important process parameter of PLD, was varied with 7×10^{-3}, 1.4×10^{-2}, and 2.8×10^{-2} torr. At last, we use ITO as a top electrode, a 100 nm-thick ITO thin film is deposited by dc sputter system using a shadow mask with a diameter of 1200 μm. Electrical characteristics were performed on Agilent 4156C semiconductor parameter analyzer (SPA) at room temperature. Current flow from the top to the bottom electrode was defined as positive sweep.

2.6 Material analyses

Material analyses are used to understand the correlation between the thin film quality and the electrical characteristics, such as X-ray diffraction, X-ray photoelectron spectrometer, atomic force microscopy, auger electron spectrometer, scanning electron microscopy, and transmission electron microscopy, which are going to be briefly introduced in the following content. The material analyses and the experimental procedures used in the thesis are summarized and shown in Fig. 2-5.

2.6.1 X-ray diffraction

The structure and crystallinity of the films were investigated by x-ray diffraction (XRD), using Siemens D-5000 diffractometer, operated with monochromatic CuKa radiation source (λ=0.1542 nm), step scanning mode with steps of 0.05° with a scan speed of 4s/step. The schematic illustrateion of the XRD is shown in Fig. 2-4. Based on the XRD theory, the average grain size of the each orientation can be calculated by using the Scherrer's formula

Where D is the average grain size of the film, λ is the wavelength of X-rays source (λ=0.1542 nm), θ is the Bragg's angle of the XRD peak, and B is the full-width at half-maximum of the peak.

2.6.2 X-ray photoelectron spectroscopy

X-ray photoelectron spectroscopy (XPS) was used to determine the HfO_x, Gd_2O_3, and LAO thin film stoichiometry and binding states. The inner electrons are excited and ionized when the light illuminates the sample surface. The ionized electrons near the surface of the matter have the ability to escape into vacuum, resulting in photoelectron. The schematic illustration of the XPS is shown in Fig. 2-5. This phenomenon is named photoelectric effect. Different components and chemical states of the matters have its specified kinetic energy, which can be used to distinguish the composition elements and the chemical binding states of the surface atoms. XPS data were collected using an Al Kα monochromatic x-ray source, 2 mm filament, 350 W power, >1 mm spot size, with electron charge neutralization and 45° takeoff angle. XPS depth profiling of the samples were performed using Ar^+ sputtering at 3 KV and 3 nA over a 4×4 mm area. The resulting data was processed using the empirically established XPS sensitivity factors provided by the instrument manufacturer to produce atomic concentration.

2.6.3 Auger electron spectrometer

Auger electron spectroscopy (AES) is a popular technique for determining the composition of the top few layers of a surface. When electron beam of energy 2-20 keV is incident upon an atom or solid surface, these electrons cause core electrons from atoms to be ejected resulting in a photoelectron and an atom with a core hole. The atom then relaxes via electrons with a lower binding energy dropping into the core hole. The energy thus released can be converted to emit an electron. This electron is called an Auger electron, and the relaxation process was discovered by Pierre Auger. The schematic illustration is shown in Fig. 2-7.

2.6.4 Atomic force microscopy

The surface topography and surface roughness of the resistive switching thin films are examined by the atomic force microscopy (AFM). First, the AFM tip is manually close to the sample surface, and then the scanner makes a final adjustment in tip-sample distance based on setpoint determined by the user. The tip in contact with the sample surface through any adsorbed gas layer, is then scanned across the sample under the action of a piezoelectric actuator, by moving the tip relative to the other. The average roughness and the root mean square are automatically recorded and calculated by the software. The schematic diagram of the AFM instrument is shown in Fig. 2-8.

2.6.5 Scanning electron microscopy

Scanning electron microscopy (SEM) is a useful method for high-resolution imaging of the surface morphology. The SEM generates a beam of incident electrons in an electron column above the sample chamber. The electrons are produced by a thermal emission source, such as a heated tungsten filament, or by a field emission cathode. The incident electrons cause electrons to be emitted from the sample due to elastic and inelastic scattering events within the sample's surface and near-surface material. The emitted electrons with high-energy by an elastic collision of an incident electron are referred to as backscattered electrons, while the emitted electrons with lower energy are resulting from inelastic scattering, which are named secondary electrons. Two electron detector types are typically used to detect the signal for SEM imaging. The schematic illustration is shown in Fig. 2-9.

2.6.6 Transmission electron microscopy

The thin film morphology including size, shape and arrangement of the particles, the thickness, the interface layer, and the crystallographic information, including the arrangement of atoms at the specific sites and detection of atomic-scale defects in a few nanometers order, can be investigated and examined by transmission electron microscopy (TEM). The TEM samples require very thin samples, typically about 100 nanometers, so the samples have to be prepared before the TEM observation. Focus ion beam (FIB) is a scientific instrument to the sample preparation for TEM investigation. Gallium (Ga+) is chosen because it is easy to build a Ga liquid metal ion source to cause the destructive sputtering onto the sample surface at the micro- and nano-scale.

After the samples preparation by FIB, then the TEM observation can be performed. The electron are accelerated from the electron fun and then focused by the condenser lenses on the sample surface. The sample is so thin and transparent enough for the incident electrons to pass through the specimen. By collecting the transmitted scattered electrons, it forms a diffraction pattern in the back focus plane and a magnified bright image in the main screen. The schematic illustration of the TEM instrument is shown in Fig. 2-9.

2.7 Electrical analyses

The electrical characteristics of various combinations of the electrodes and the resistive switching films are performed by the semiconductor parameter analyzer (Agilent 4156C). All the measurement instruments are controlled by a computer with the assistant of the Agilent VEE software. The electrical characteristics of the device are performed by applying a specific sweep voltage. The voltage source is applied on the top electrode while the bottom electrode is grounded. Fig. 2-10 shows the measuring schematic diagram of the Agilent 4156C.

2.7.1 Current-voltage measurement

The I-V characteristics of the metal-insulator-metal (MIM) capacitor structure are performed by Agilent 4156C. The basic resistive switching behavior is based on the different conductivity of the memory device which was triggered by applying a specific voltage. Once the switching properties are reproducible, we refer it as the resistive memory. Unipolar and bipolar resistive switching are the two basic operation type which are performed by the same voltage bias and the opposite voltage bias, respectively. Under the unipolar operation, a current compliance is needed to protect the memory device from hard breakdown, while the bipolar switching is sometimes not, depending on the material used.

In the investigation of the plasma effect in section 3.3.5, we also adapted the current mode (CM) operation to investigate the variation of the measured voltage. The CM operation indicates that applied current bias is used while measuring the voltage values, which is contrary to the general measurement named voltage mode (VM) discussed above. CM operations can reveal information unobservable in VM operation, so it is a powerful measurement to explore the unknown.

2.7.2 Retention time test

The data retention is the time that the stored information can be maintained without any power supply. This test is also measured by the Agilent 4156C. Before the measurement, two identical devices are switched to high or low resistance states, respectively. Then, a small voltage value, which is not large enough to disturb the state, was used to test the retention time. Sometimes, the retention time is also tested under a high temperature circumstance to perform the thermal acceleration test.

2.7.3 Endurance test

The endurance is the number that the memory device can be switched between high and low resistance state reproducibly by applying a sweeping voltage or pulsed voltage. For a stable and reliable usage, the switching cycles of the memory devices are expected to be as large as possible. The endurance test was performed on Agilent 4156C with an automatic measurement setup by repeatedly applying voltage values, and then read the current values at certain voltage (about 0.1 V).

2.7.4 Readout test

The read disturb immunity of the stored data is tested by applying constant voltage stress and reading the current value of the MIM structure. The maximum read times and the stability of the memory cells can be determined from the experimental results.